IMPLEMENTATIONS OF QUANTUM RANDOM WALKS

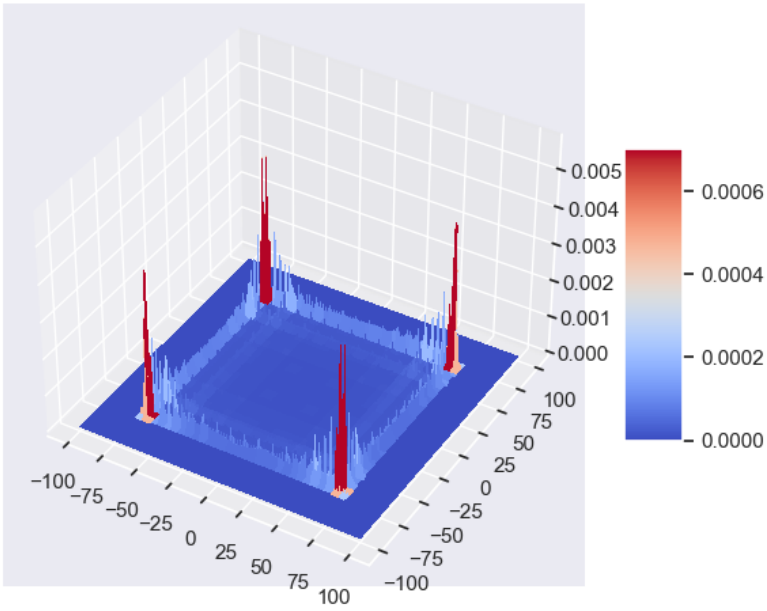

BSc thesis Applied Physics and Applied Mathematics

by

Anne-Fleur DIJKHORST

TU Delft Delft University of Technology

Supervisors:

Prof.dr. B.M. Terhal Dr. J.L.A. Dubbeldam

Other committee members:

Prof.dr. A.F. Otte Dr. B. Janssens

ABSTRACT

In this research, the implementations of quantum random walks in superconducting circuit-QED are studied. In particular, a walk that moves across the Fock states of a quantum harmonic oscillator by a Jaynes-Cummings model is investigated, which is difficult to implement because of different Rabi frequencies Ω_n for different Fock states. Theoretically, the lower boundary vacuum state of the harmonic oscillator causes a reflection of the probability amplitudes in the distribution. A walk that moves across a grid of coherent states $|n\alpha + im\alpha\rangle$ in phase space is then investigated. A setup for a 1D and 2D quantum random walk is suggested, using controlled displacements of a resonator dispersively coupled to one or two superconducting transmon qubits in circuit-QED, followed by Hadamard gates. From numerical simulations it was observed that the 2D walk commutes for $\alpha \cdot \beta = 0 \bmod \frac{\pi}{2}$ for which the variance has proportionality $\sigma_x^2 \sim t^2$. For other values of $\alpha \cdot \beta$ the horizontal and vertical displacements do not commute, resulting in extra phase factors. The numerical simulations showed that for most values of $\alpha \cdot \beta$ with a larger distance to 0 mod $\frac{\pi}{2}$ than 0.01, the probability distribution of the walk collapses to a distribution centered around origin within $t = 100$ steps, similar to a classical random walk. Exceptions are the 2D walks for $\alpha \cdot \beta = \pm\frac{\pi}{6} \bmod \frac{\pi}{2}$ or $\pm\frac{\pi}{4} \bmod \frac{\pi}{2}$, which still show proportionality $\sigma_x^2 \sim t^2$.

CONTENTS

Abstract i

1 Introduction 1

2 Introduction to quantum random walks 2

2.1 Classical random walks . . . 2

2.1.1 Discrete classical random walks . . . 2

2.1.2 Applications of classical random walks . . . 6

2.2 Quantum mechanics, an overview . . . 6

2.2.1 The Schrödinger equation . . . 6

2.2.2 The wave function, probabilities and measurements . . . 7

2.2.3 The time-independent Schrödinger equation . . . 7

2.2.4 Unitarity . . . 8

2.2.5 Bra-ket notation . . . 8

2.2.6 Quantum bits (qubits) . . . 8

2.3 Quantum random walks . . . 9

2.3.1 Discrete quantum random walks. . . . 9

2.3.2 Summary of important differences between classical and quantum random walks . . . 14

2.3.3 Applications of quantum random walks . . . 14

3 The quantum random walk on a harmonic oscillator 15

3.1 The quantum harmonic oscillator . . . 15

3.2 The Jaynes-Cummings Hamiltonian 17
3.2.1 Quantization of the electromagnetic field 17
3.2.2 The Jaynes-Cummings model 18
3.3 Physical implementations of the QRW 22
3.3.1 Trapped ions 23
3.3.2 Cavity and circuit quantum electrodynamics 23
3.4 Implementation of the QRW on the Fock states of a harmonic oscillator . . 23

4 Implementation of the quantum random walk on superconducting circuit-QED in phase space 27

4.1 The displacement operator and coherent states 27
4.1.1 Controlled displacements by rotations 29
4.2 1D quantum random walk with controlled displacements 31
4.3 2D quantum random walks with controlled displacements 31
4.3.1 Derivation of the coefficients of the recursive walk in 2D 32
4.3.2 Results of commuting quantum random walks on the 2D grid in phase space 35
4.3.3 Results of noncommuting quantum random walks on the 2D grid in phase space 37

5 Discussion 44

5.1 Discussion of physical limitations of the implementation of a QRW in phase space 44
5.2 Suggestions for further research 45

6 Conclusion 47

A Appendix: Link to numerical code 51

1

INTRODUCTION

Classical random walks have been applied in many useful applications and algorithms. [1] With the upcoming of the quantum computer, a quantum counterpart of the classical random walk called the quantum random walk has been proposed in 1993. [2] Research on the properties of this quantum random walk and quantum walk based algorithms has shown promising results indicating that the quantum random walk outperforms its classical counterpart. [1]

In this thesis we investigate the implementation of quantum random walks on physical systems that may later form the building blocks of the quantum computer. In what ways is an implementation of a quantum random walk on a physical system realizable? Which properties of the quantum random walks arise in these setups? We focus on implementations in superconducting circuit-QED. [3] In particular, we investigate a quantum random walk that moves between the Fock states of a harmonic oscillator and a quantum walk that moves between coherent states in phase space of an oscillator.

In Chapter 2 an introduction is given on classical random walks and their applications, after which we introduce the definitions, advantages and applications of a quantum random walk. The theory behind the implementation of the walk in a physical system is given in Chapter 3, where the quantum harmonic oscillator and the Jaynes-Cummings model are studied. In this chapter the implementation of the walk on the Fock states of a harmonic oscillator is investigated. In Chapter 4 the implementation and numerical results of the walk on coherent states are studied, after which a discussion and conclusion of the research is presented in Chapter 5 and Chapter 6. A link to the numerical code used throughout the chapters may be found in Appendix A.

This research is done as a BSc thesis for the BSc Applied Physics and BSc Applied Mathematics at the faculties of Applied Sciences and Electrical Engineering, Mathematics and Computer Science at the Delft University of Technology.

2

INTRODUCTION TO QUANTUM RANDOM WALKS

In this chapter an introductory overview is given on quantum random walks. First a mathematical description and known results of discrete time classical random walks will be introduced, after which we will study the applications of classical random walks. A very basic overview of quantum mechanics that is needed to understand the description of a quantum random walk will be given, after which the definitions and results of discrete time quantum random walks are shown. Finally a few examples of applications and advantages of quantum random walks will be mentioned.

2.1. CLASSICAL RANDOM WALKS

A Classical Random Walk (CRW) is a process consisting of a repeated sequence of random steps in some mathematical space. This mathematical space could for example be the integers $\mathbb{Z}$, a d-dimensional space such as a two-dimensional grid or cubic lattice, or a graph where the walk moves across the vertices. In natural phenomena random walks are for example seen in the path traveled by a molecule in a gas or liquid, which we call Brownian motion, or in genetic drift of a population. Random walks are increasingly popular in mathematics and computer science because of their applications in algorithms and models. [1]

2.1.1. DISCRETE CLASSICAL RANDOM WALKS

In a discrete CRW model, the random walk is localized at some discrete point in a mathematical space and has a probability to jump to another position in the next discrete step according to a probability distribution. Mathematically this can be denoted as $\xi_t, t = 0, 1, 2, ...$, where ξ_t is the random variable that describes the position of the ran-

dom walk at time t. The probability distribution of the position of the random walk at time t is then given by $P_t(i) = P(\xi_t = i)$, where i is a position in the position space of the random walk. A transition probability $p_{i\to j} = P(\xi_{t+1} = j|\xi_t = i)$, with $\sum_j p_{i\to j} = 1$ gives the probability that the random walk moves from the position i to j in the step from t to $t+1$. [1] We study a few cases of the discrete CRW.

CLASSICAL RANDOM WALK ON THE 1D LINE OF INTEGERS

The state space of the CRW on the one-dimensional line of integers is given by the points $\{i : i \in \mathbb{Z}\}$. The walk starts at a position $i = \xi_0 \in \mathbb{Z}$ and has the following transition probability in each time step:

$$p_{i\to j} = \begin{cases} p & \text{if } j = i+1, \\ 1-p & \text{if } j = i-1, \\ 0 & \text{otherwise.} \end{cases} \tag{2.1}$$

Intuitively this corresponds to throwing a p-biased coin at each step of the walk to decide if the walk moves one position to the right with probability p, or to the left with probability $1-p$ on the line of integers. A specific case of the walk on the line of integers is the symmetric walk where we choose $p = \frac{1}{2}$. An example of a realization of the simple symmetric random walk starting at position $\xi_0 = 0$ for 100 steps is shown in Figure 2.1. Here it is clear to see that the walk has not propagated far from its initial position in the 100 steps (the walk is at 3 steps away from 0 at $t = 100$).

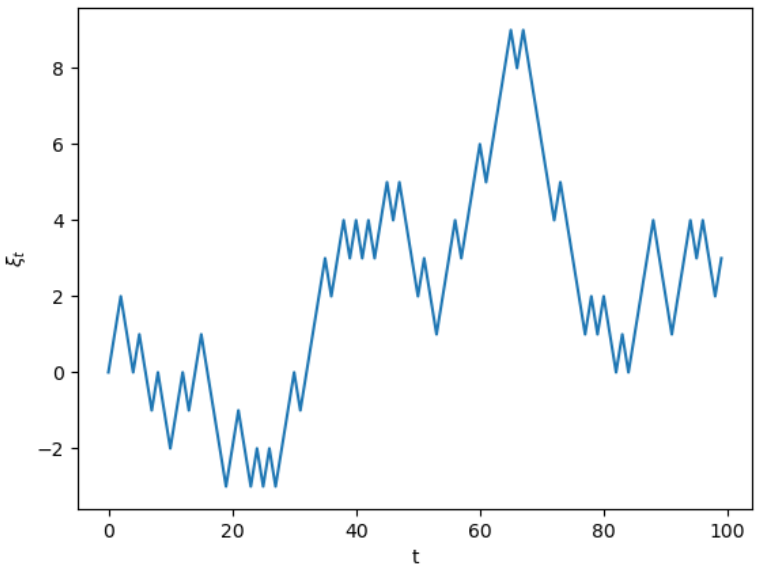

Figure 2.1: A single realization of the symmetric CRW on the 1D line of integers for 100 steps.

The probability distribution at a time $t = T$ of this motion is given by the random variable $\xi_T = \sum_{t=0}^{T} X_t$ where the X_t's are independent random variable with $P(X_t = 1) = p$, $P(X_t = -1) = 1 - p$. The expected value of the position of the random walk at time t is then given by

$$E[\xi_T] = E[\sum_{t=0}^{T} X_t] = \sum_{t=0}^{T} E[X_t] = -1 + 2p, \tag{2.2}$$

and the variance of the position of the random walk at time t is given by

$$\sigma_x^2(t) = E[(\xi_t - E[\xi_t])^2] = E[\xi_t^2] = \sum_{t=0}^{t} E[X_t^2] = t. \tag{2.3}$$

By central limit theorem it follows that this distribution approaches a standard normal distribution with $\mu = 0$ and $\sigma_x^2 = t$ for large t. [4] We can find the probabilities of the symmetric case of the walk by the following recursive formula:

$$P_t(i) = \frac{1}{2}P_{t-1}(i-1) + \frac{1}{2}P_{t-1}(i+1), \tag{2.4a}$$

$$P_0(i) = \begin{cases} 1 & \text{if } i = 0, \\ 0 & \text{otherwise.} \end{cases} \tag{2.4b}$$

This distribution of the CRW with initial position $\xi_0 = 0$ for 100 steps on the integers is plotted in Figure 2.2, where only nonzero values are plotted. The variance of the CRW with initial position $\xi_0 = 0$ is plotted against the number of steps in Figure 2.3.

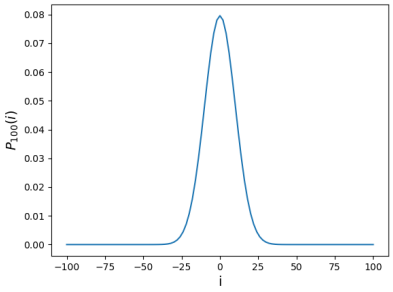

Figure 2.2: Probability distribution of the 1D CRW on the integers after 100 steps, with initial position $\xi_0 = 0$.

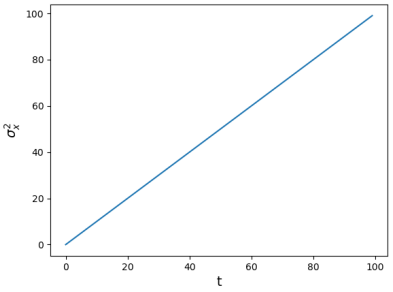

Figure 2.3: Variance of the 1D CRW on the integers plotted against number of steps, with initial position $\xi_0 = 0$.

CLASSICAL RANDOM WALK ON THE 2D GRID

The discrete CRW on the one-dimensional line of integers is easily extended to the 2D CRW on a grid. The state space is now given by the coordinates $\{(i, j) : i, j \in \mathbb{Z}\}$. Instead of a coin with two sides we may now intuitively imagine throwing a 4-sided dice with probabilities p_1, p_2, p_3, p_4 corresponding to each direction in which the walk can move,

such that $\sum_{i=1}^{4} p_i = 1$. The symmetric case is then $p_i = \frac{1}{4} \forall i$. We will now study the results for a walk that moves from a position (i, j) to the positions $(i \pm 1, j \pm 1)$ in one step, for reasons which will become clear later on in this research. Of course it is also possible to investigate a walk that moves to the positions $(i \pm 1, j), (i, j \pm 1)$ in a step.

We can find the probabilities for the 2D CRW on the grid by the recursive formula

$$\begin{aligned} P_t(i,j) = \frac{1}{4}\big(&P_{t-1}(i-1,j-1) + P_{t-1}(i-1,j+1) \\ &+ P_{t-1}(i+1,j-1) + P_{t-1}(i+1,j+1)\big) \end{aligned} \tag{2.5a}$$

$$P_0(i,j) = \begin{cases} 1 & \text{if } i,j = 0, \\ 0 & \text{otherwise.} \end{cases} \tag{2.5b}$$

A heat map of the probability distribution of the CRW on the 2D grid with initial position $\xi_0 = (0,0)$ after 100 steps is given in Figure 2.4. The evolution of the probability distribution during the 100 steps is shown in a linked animated movie.

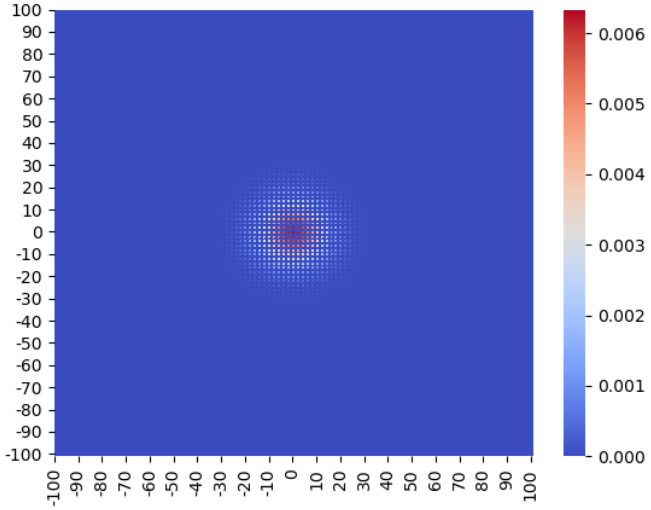

Figure 2.4: Heatmap of the probability distribution of the 2D CRW after 100 steps with initial position $\xi_0 = (0,0)$.

The probability distribution for this walk can also be found from the probability distribution for the CRW on the 1D line of integers by

$$P_t(i,j) = P_t(i)P_t(j). \tag{2.6}$$

Therefore, the variance of the x and y coordinates of the 2D walk is equal to the variance of the 1D walk.

CLASSICAL RANDOM WALK ON A GRAPH

The CRW may also be performed on a connected and undirected graph $G = (V, E)$, where V is the set of vertices of size $|V| = N$ which forms the state space of the CRW, and E is the set of edges which correspond to transitions between steps of the walk. Let $A \in \mathbb{R}^{N\times N}$ be the adjacency matrix of G such that

$$A_{ij} = \begin{cases} 1 & \text{if } e = \{i, j\} \in E, \\ 0 & \text{otherwise.} \end{cases} \tag{2.7}$$

The degree d_i of a vertex, which gives the number of neighbours of a vertex equals $\sum_j A_{ij}$. For a simple random walk we say that the probability for the walk to move from vertex i to a neighbour of i is equal to $\frac{1}{d_i}$. In the simplest case we consider a d-regular graph, where each vertex has degree d. The transition matrix $W_d = \frac{1}{d}A$ (for which we know that $\sum_j W_{ij} = 1, \forall i$) gives the transitions in each step. The probability distribution of the walk over the vertices of the graph is then given by the vector $\vec{P}_t = W_d^t \vec{P}_0$, where the i^{th} element of the vector gives the probability $P_t(i)$. For connected and non-bipartite graphs it is known that the distribution $\vec{P}_t$ converges to a stationary distribution $\vec{\pi}$ which is independent of the initial distribution $\vec{P}_0$ of the walk. For a d-regular graph it is known that the limiting probability distribution $\vec{\pi}$ is uniform over the vertices of the graph. [5]

2.1.2. APPLICATIONS OF CLASSICAL RANDOM WALKS

CRW's have several applications in algorithms. [1] CRW's are for example a tool for analysing complex networks. An example of such a network is the network of web pages in the World Wide Web. This is an enormous network with many nodes and directed edges which represent hyperlinks from one page to another. The PageRank algorithm [6] used by Google to rank the pages on the web is a random walk based algorithm. The property that a CRW converges to a stationary distribution $\vec{\pi}$ under the right circumstances may be used to examine properties and analyse the topology of a complex network by sampling from $\vec{\pi}$. Another application of the CRW is a random walk based cards shuffle algorithm. [7] A problem with CRW based algorithms is the time complexity for large state spaces.

2.2. QUANTUM MECHANICS, AN OVERVIEW

In this section a short overview of quantum mechanics [8] is given that is needed for the theory of a quantum random walk that will be given afterwards.

2.2.1. THE SCHRÖDINGER EQUATION

In classical mechanics we use Newton's equations to describe the motion of particles. In quantum mechanics the Schrödinger equation replaces this role. The Schrödinger equation for a particle in a specified potential V is given by

$$i\hbar\frac{\partial\Psi}{\partial t} = -\frac{\hbar^2}{2m}\frac{\partial^2\Psi}{\partial x^2} + V\Psi, \tag{2.8}$$

where $\hbar$ is Planck's constant, Ψ is the wave function that describes the motion of the particle and m is the mass of the particle.

2.2.2. THE WAVE FUNCTION, PROBABILITIES AND MEASUREMENTS

An important difference between quantum mechanics and classical mechanics is the way we describe particles. In classical mechanics we describe a particle at a determined location which is no longer the case in quantum mechanics. We now consider a particle's *wave function*, most commonly denoted by $\Psi(x,t)$. The wave function can be obtained by solving the Schrödinger equation. The interpretation of the wave function is that $|\Psi(x,t)|^2$ gives the probability to measure the particle at position x for a time t. Because of this, it is required for a wave function that

$$\int_{-\infty}^{\infty} |\Psi(x,t)|^2 dx = 1. \tag{2.9}$$

Therefore it is necessary to normalize a wave function that is obtained from solving the Schrödinger equation so the above property is satisfied.

Before performing a measurement of a quantity of a particle, such as energy, momentum or position, we only know the probability that a quantity will take a certain value. When a measurement is performed, we say that the wave function *collapses* to a sharp peak around the measured value of the quantity.

2.2.3. THE TIME-INDEPENDENT SCHRÖDINGER EQUATION

By performing separation of variables on the time-dependent Schrödinger equation in Equation (2.8) we obtain *a time-independent Schrödinger equation*, which is given by

$$-\frac{\hbar^2}{2m}\frac{d^2\psi(x)}{dx^2} + V\psi(x) = E\psi(x), \tag{2.10}$$

which is also often written as,

$$\hat{H}\psi = E\psi \tag{2.11}$$

where $\hat{H} = \frac{\hat{p}^2}{2m} + V(x)$ is the Hamiltonian operator and $\hat{p} = \frac{\hbar}{i}\frac{\partial}{\partial x}$ is the momentum operator. Solutions to the time-independent Schrödinger equation give rise to *stationary states* or *eigenstates* of the system. The probability density of these states does vary not over time. The time dependence of these states is then included by using the time-dependent Schrödinger equation which we may also write in a form using the Hamiltonian:

$$i\hbar\frac{d}{dt}\Psi(x,t) = \hat{H}\Psi(x,t) \tag{2.12}$$

from which it follows that the time dependence of a stationary state is given by

$$\Psi(x,t) = \Psi(x,0)e^{-iEt/\hbar}. \tag{2.13}$$

2.2.4. UNITARITY

For general states, the operator $\hat{U} = e^{-i\hat{H}t/\hbar}$ gives the time evolution of a system that evolves under a Hamiltonian $\hat{H}$. This operator $\hat{U}$ is *unitary*. That is,

$$\hat{U}\hat{U}^\dagger = \hat{U}^\dagger\hat{U} = I. \tag{2.14}$$

The unitarity of the operator guarantees that inner products are preserved which is important in quantum mechanics since we are calculating with probabilities. The sum of probabilities equal to 1 is conserved in unitary transformations.

2.2.5. BRA-KET NOTATION

In quantum mechanics the posssible states of a particle or a system are linear combinations of unit vectors in a complex Hilbert space. These states are often denoted as $|\Psi\rangle$. We call this notation $|.\rangle$ a *ket*. The ket represents a column vector. If the Hilbert space containing all possible states of the system is spanned by the orthogonal basis of vectors $|\psi_1\rangle, ..., |\psi_n\rangle$ then a state $|\Psi\rangle$ can be written as a linear combination of $|\psi_i\rangle$'s: $|\Psi\rangle = c_1|\psi_1\rangle + ... + c_n|\psi_n\rangle$, where $\sum_{i=1}^{n} |c_i|^2 = 1$ such that the probability to measure any of the states $|\psi_i\rangle$ adds up to 1. The Hermitian conjugate of the ket is denoted as $\langle\Psi|$, such that the inner product between two states may be written as $\langle\phi|\psi\rangle$. We call this Hermitian conjugate $\langle.|$ a *bra*. For an orthogonal basis $|\psi_1\rangle, ..., |\psi_n\rangle$, we have that $\langle\psi_i|\psi_j\rangle = \delta_{ij}$.

2.2.6. QUANTUM BITS (QUBITS)

Classical bits of a computer are in a state 0 or 1. In quantum computation a *quantum bit (qubit)* [9] is used, which is in a superposition of states 0 and 1. This may be denoted as

$$|\psi\rangle = \alpha|0\rangle + \beta|1\rangle, \tag{2.15}$$

where $\alpha, \beta \in \mathbb{C}$ and $|\alpha|^2 + |\beta|^2 = 1$. $|\alpha|^2$ gives the probability that the qubit is measured in a state $|0\rangle = [1,0]^T$ and $|\beta|^2$ gives the probability that the qubit is measured in the state $|1\rangle = [0,1]^T$. A qubit is often visually represented by a vector pointing from the center to the surface of a unit sphere. We call this the *Bloch sphere*.

In quantum computation, the state of a qubit can be transformed by applying *single qubit gates* to the qubit. Mathematically a single qubit gate may be represented by 2×2 matrices. In the Bloch sphere representation of the qubit these gates correspond to rotations of the qubit vector on the sphere. A few commonly used single qubit gates are the Pauli gates $\hat{\sigma}_x, \hat{\sigma}_y, \hat{\sigma}_z$, also often referred to as X, Y, Z. The Pauli-matrices are given

by

$$\hat{\sigma}_x = X = \begin{bmatrix} 0 & 1 \\ 1 & 0 \end{bmatrix},$$
$$\hat{\sigma}_y = Y = \begin{bmatrix} 0 & -i \\ i & 0 \end{bmatrix}, \tag{2.16}$$
$$\hat{\sigma}_z = Z = \begin{bmatrix} 1 & 0 \\ 0 & -1 \end{bmatrix}.$$

It is also possible to apply *multiple-qubit gates* to several qubits simultaneously. Mathematically these gates are represented by $2N \times 2N$-matrices, where N is the number of qubits. There are several two-level physical systems that behave as a qubit and might be used as a building block of a quantum computer. We will study this shortly in Chapter 3.

2.3. QUANTUM RANDOM WALKS

We will now use the probabilistic behaviour of particles in quantum mechanics to describe a new model of the CRW that is called the Quantum Random Walk (QRW). Instead of moving in a deterministic path from one position to another, the QRW moves in superposition in each possible direction, allowing for interference. QRW's were first introduced by Aharonov et al. [2] in 1993.

We will again first study a 1D QRW, after which we extend the technique to a 2D grid. Just as for the CRW's, we consider discrete time QRW's.

2.3.1. DISCRETE QUANTUM RANDOM WALKS

The discrete QRW [10] moves in discrete steps on discrete positions on a line or graph, just like the discrete CRW. The idea is similar to the discrete CRW, however, we need an extra auxiliary space to perform the discrete QRW.

POSITION STATE SPACE

We will describe the possible positions of the QRW as orthonormal basis states which we denote as $|i\rangle, i \in \mathbb{Z}$. These states span a position Hilbert Space $\mathscr{H}_P = \{|i\rangle : i \in \mathbb{Z}\}$ for an infinite number of discrete positions or $\mathscr{H}_P = \{|i\rangle : i \in \{0, ..., N-1\}\}$ for a walk on a finite space with N possible discrete positions.

COIN STATE SPACE

To describe a discrete QRW we make use of an extra Hilbert space $\mathscr{H}_C$ that we may call the "coin"-space. The possible coin states that span $\mathscr{H}_C$ are intuitively equivalent to the two sides of a coin (when the walk has $d = 2$ possible directions to walk from each discrete position) or as sides of a d-faced dice (when there are $d \in \mathbb{N}$ directions to walk in). These states are denoted as $\left|j\right\rangle \forall\, j \in \{1, ..., d\}$ and are again orthonormal basis states.

The total state of the walk is denoted as a tensor product of a position state and a coin state: $|i\rangle \otimes \left|j\right\rangle$. In some cases we may write the tensor product shorter as $\left|i, j\right\rangle$.

In the discrete model, a single step of the QRW consists of two sub-steps. We first transform the coin state of the walk and then perform a conditional shift in position.

DISCRETE QUANTUM RANDOM WALK IN 1D

We will now show how the walk on a one-dimensional infinite line is described. The position Hilbert Space represents the integer numbers on the infinite line $\mathcal{H}_P = \{|i\rangle : i \in \mathbb{Z}\}$. On the one-dimensional line, there are two possible positions to walk to from each $|i\rangle$; $|i-1\rangle$ and $|i+1\rangle$. Therefore we need two coin states, corresponding to each direction. When there are two possible coin states, they are often denoted as $\{|\uparrow\rangle, |\downarrow\rangle\}$, with analogy to a spin-$\frac{1}{2}$-particle such as a qubit. The coin states are also often denoted as $\{|0\rangle, |1\rangle\}$, which we will use in this research as a convention.

To make sure that the walk moves in superposition to each side, we want to transform a state $\{|0\rangle$ of the coin into $a|0\rangle + b|1\rangle$. A commonly used unitary coin operator is the Hadamard coin H. The Hadamard gate is

$$H = \frac{1}{\sqrt{2}}\begin{pmatrix} 1 & 1 \\ 1 & -1 \end{pmatrix}. \tag{2.17}$$

H transforms the coin states $|0\rangle, |1\rangle$ as follows:

$$\begin{aligned} H|0\rangle &= \frac{1}{\sqrt{2}}(|0\rangle + |1\rangle) = |+\rangle \\ H|1\rangle &= \frac{1}{\sqrt{2}}(|0\rangle - |1\rangle) = |-\rangle. \end{aligned} \tag{2.18}$$

The coin is balanced; measuring the coin state after applying the operator H to any of the coin states $|0\rangle, |1\rangle$ results in $1/2$ probability for each of the coin states. There are other possibilities for unitary, balanced coin operators. We will use the Hadamard coin.

After applying the coin operator $C(= H)$, we want to apply a conditional shift operator S that transforms an initial state $|i\rangle \otimes |0\rangle$ to $|i+1\rangle \otimes |0\rangle$, and initial state $|i\rangle \otimes |1\rangle$ to $|i-1\rangle \otimes |1\rangle$.

The following unitary operator performs this shift:

$$S = \sum_i |i+1\rangle\langle i| \otimes |0\rangle\langle 0| + \sum_i |i-1\rangle\langle i| \otimes |1\rangle\langle 1| \tag{2.19}$$

To summarize, we first apply the Hadamard operator only to the coin state to create a superposition of directions in which the walk will transform, thus by applying the operator $I \otimes C$ to the initial state $|i\rangle \otimes |j\rangle = |i,j\rangle$. Then we apply the shift operator S to $(I \otimes C)|i,j\rangle$. Thus the total operator we use to perform a step in two directions for each discrete time step is defined as

$$U = S(I \otimes C). \tag{2.20}$$

Therefore we can describe the state of a walk that was initially in the state $|\Psi_0\rangle$ after t time steps as

$$|\Psi_t\rangle = U^t |\Psi_0\rangle . \tag{2.21}$$

The probability to measure the walk in the position $|i\rangle$ is now given by

$$P_t(i) = |\langle i,0|\Psi_t\rangle|^2 + |\langle i,1|\Psi_t\rangle|^2. \tag{2.22}$$

We can find the probability distribution of the walk after t steps in a recursive way. It is a general convention is to write the walk as in Equation (2.20). In most derivations in this research we used the different convention $U = (I \otimes C)S$), which overall does not matter for the evolution of the walk. Using this convention, we write the unitary operator U as

$$U = \sum_i |i+1\rangle\langle i| \otimes |+\rangle\langle 0| + \sum_i |i-1\rangle\langle i| \otimes |-\rangle\langle 1| \tag{2.23}$$

From this we can see that the operator U^t will be of the form

$$U^t = \left(\frac{1}{\sqrt{2}}\right)^{t-1}\left(D^t_{+0} \otimes |+\rangle\langle 0| + D^t_{+1} \otimes |+\rangle\langle 1| + D^t_{-0} \otimes |-\rangle\langle 0| + D^t_{-1} \otimes |-\rangle\langle 1|\right) \tag{2.24}$$

with $D_{\pm j} = \sum_n c^t_{n,\pm j} \sum_i |i+n\rangle\langle i|$. By calculating how U^{t+1} follows from U^t we may find how the coefficients $c^{t+1}_{n,\pm j}$ can be calculated from the $c^t_{n,\pm j}$'s as follows:

$$\begin{aligned}
c^{t+1}_{n,+0} &= c^t_{n-1,+0} + c^t_{n-1,+1} \\
c^{t+1}_{n,+1} &= c^t_{n-1,-0} + c^t_{n-1,-1} \\
c^{t+1}_{n,-0} &= c^t_{n+1,+0} - c^t_{n+1,+1} \\
c^{t+1}_{n,-1} &= c^t_{n+1,-0} - c^t_{n+1,-1}
\end{aligned} \tag{2.25}$$

where we have that

$$\begin{aligned}
c^1_{n,+0} &= \begin{cases} 1 & \text{for } n = 1, \\ 0 & \text{otherwise.} \end{cases} \\
c^1_{n,+1} &= 0 \\
c^1_{n,-0} &= 0 \\
c^1_{n,-1} &= \begin{cases} 1 & \text{for } n = -1, \\ 0 & \text{otherwise.} \end{cases}
\end{aligned} \tag{2.26}$$

The state $|\Psi_t\rangle$ of the walk with initial position $|\Psi_0\rangle = |x_0\rangle \otimes (a|0\rangle + b|1\rangle)$ is then given by

$$U^t |\Psi_0\rangle = \left[\frac{1}{\sqrt{2}}\right)^{t-1}\left(a\left(D^t_{+0}|x_0\rangle \otimes |+\rangle + D^t_{-0}|x_0\rangle \otimes |-\rangle\right) + b\left(D^t_{+1}|x_0\rangle \otimes |+\rangle + D^t_{-1}|x_0\rangle \otimes |-\rangle\langle 1|\right)\right]. \tag{2.27}$$

Using that $\langle x_0+n|\, D^t_{\pm j}\,|x_0\rangle = c^t_{n,\pm j}$ and Equation (2.28) we find that the probability to measure the walk with initial position $|\Psi_0\rangle$ after t in the position $|x_0+n\rangle$ is obtained by

$$\begin{aligned} P_t(x_0+n) =& |\langle 0, x_0+n|\Psi_t\rangle|^2 + |\langle 1, x_0+n|\Psi_t\rangle|^2 = \\ & \frac{1}{2^t}\Big(|a\big(c^t_{n,+0}+c^t_{n,-0}\big)+b\big(c^t_{n,+1}+c^t_{n,-1}\big)|^2 \\ & +|a\big(c^t_{n,+0}-c^t_{n,-0}\big)+b\big(c^t_{n,+1}-c^t_{n,-1}\big)|^2\Big). \end{aligned} \tag{2.28}$$

The fact that the walk simultaneously moves in each direction results in effects that are radically different from the CRW, which we can already see from the recursive coefficients of the walk where addition and subtraction in the coefficients shows constructive and destructive interference of the walk.

Suppose the initial state of the walk is $|\Psi_0\rangle = |0\rangle\otimes|0\rangle$. A plot of the 1D QRW after 100 steps is shown in Figure 2.5. The first thing we notice is an asymmetry, which arises because

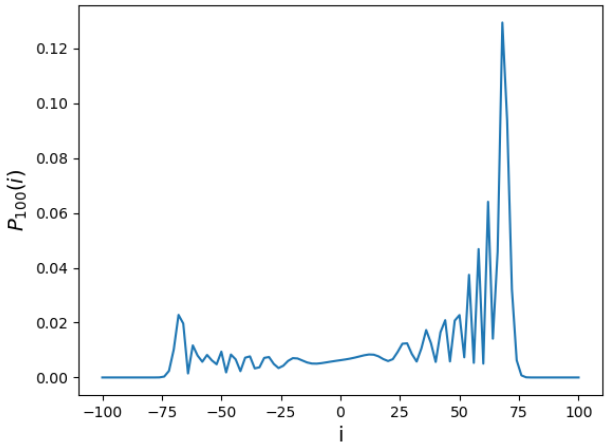

Figure 2.5: Probability distribution of the one-dimensional QRW on the integers after 100 steps, with initial state $|0\rangle\otimes|0\rangle$.

the Hadamard coin treats the states $|0\rangle$ and $|1\rangle$ differently. Interference arises, where the probability amplitudes of the positions to the left are destructively interfered and the probability amplitudes of the positions to the right are constructively interfered. If we choose $|\Psi_0\rangle = |0\rangle\otimes|1\rangle$, we obtain the distribution in Figure 2.5 but then mirrored in $i=0$. If we then choose an initial state $|\Psi_0\rangle = |0\rangle\otimes\frac{1}{\sqrt{2}}\big(|0\rangle + i\,|1\rangle\big)$, the asymmetry does not arise. This is because the Hadamard operator does not introduce any complex amplitudes, such that two walks emerging from initial coin states $|0\rangle$ and $|1\rangle$ do not interfere. The 1D QRW after 100 steps with this symmetric initial state $|\Psi_0\rangle$ is shown in Figure 2.6 together with the CRW in 1D for 100 steps plotted in red.

From the plot we can easily see that the expected value of the position of the walk is equal to 0, just like for the CRW. A significant difference between the two walks is the single peaked distribution of the CRW, compared to a double peaked distribution of the QRW. In this thesis we will mainly study symmetric cases of the QRW such that we can study the variance of the walk as a measure of how far the walk has propagated. The variance of the symmetric 1D QRW is plotted against the number of steps in Figure 2.7, together with the variance of a 1D CRW. Clearly, the QRW propagates much faster than the CRW. In fact, for the QRW $\sigma_x^2 \sim t^2$. This property makes the QRW an interesting tool in algorithmic applications, which we will shortly study at the end of this chapter.

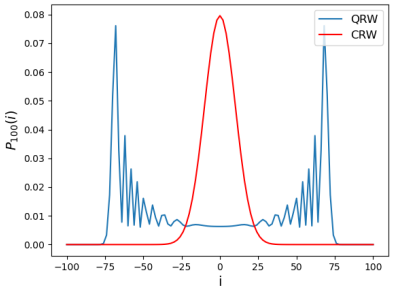

Figure 2.6: Probability distribution of the one-dimensional CRW (in red) and QRW (in blue) on the integers after 100 steps, with symmetric initial state $|0\rangle \otimes (|0\rangle + i|1\rangle)/\sqrt{2}$. Only nonzero values of both distributions are plotted.

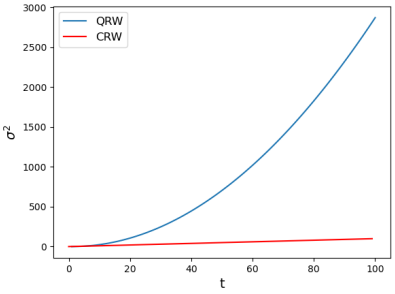

Figure 2.7: Variance of the one-dimensional CRW (in red) and QRW (in blue) on the integers plotted against number of steps, with symmetric initial state.

DISCRETE QUANTUM RANDOM WALK ON THE 2D GRID

The discrete QRW on the 1D line may be extended to the 2D grid in a similar way to the CRW on the 2D grid. However, we now need extra coin states because the walk moves in 4 directions at each step of the walk. There are several options to choose for these coin states, but for simplicity we will choose two coins (qubits) such that the four coin states are $|00\rangle, |01\rangle, |10\rangle$ and $|11\rangle$, where in each step we perform two Hadamard operators, one for each of the coins. The first qubit corresponds to a movement to the left for $|0\rangle_1$ and to the right for $|1\rangle_1$. The second qubit corresponds to a movement up for $|0\rangle_2$ and down for $|1\rangle_2$. The walk then moves from a position state $|n,m\rangle$ to $|n\pm1, m\pm1\rangle$ using the following unitary operator:

$$\begin{aligned} U = &\sum_{n,m} |n+1, m+1\rangle\langle n,m| \otimes |++\rangle\langle 00| + \sum_{n,m} |n+1, m-1\rangle\langle n,m| \otimes |+-\rangle\langle 01| \\ &+ \sum_{n,m} |n-1, m+1\rangle\langle n,m| \otimes |-+\rangle\langle 10| + \sum_{n,m} |n-1, m-1\rangle\langle n,m| \otimes |--\rangle\langle 11|. \end{aligned} \tag{2.29}$$

Properties of this 2D QRW will extensively be studied in Chapter 4 of this thesis.

2.3.2. SUMMARY OF IMPORTANT DIFFERENCES BETWEEN CLASSICAL AND QUANTUM RANDOM WALKS

An important difference between a CRW and QRW is the proportionality of the variance with the number of steps of the walk. We have seen that $\sigma_x^2 \sim t$ for a CRW in 1D and $\sigma_x^2 \sim t^2$ for a QRW in 1D. This indicates that the QRW propagates faster than the CRW.

We shortly studied the CRW on a graph, for which we know that under the right circumstances this CRW will converge to a stationary distribution $\vec{\pi}$. For QRW's this is not the case in general. Let $|\Psi_0\rangle$ be the initial state of the walk. The state of the walk at time t is then given by $|\Psi_t\rangle = U^t|\Psi_0\rangle$. The limit $\lim_{t\to\infty}|\Psi_t\rangle$ does not exist in general, because U is a unitary operator which should always be invertible. Therefore a different probability distribution is considered. We use the following distribution:

$$P_t(v \mid \Psi_0) = \sum_j \left|\langle j, v \mid \Psi_t\rangle\right|^2, \tag{2.30}$$

which gives the probability to measure the walk at a vertex v at time t, given an initial state $|\Psi_0\rangle$, where we sum over all possible coin states j. This distribution still does not converge, but its average

$$\overline{P}_T(v \mid \Psi_0) = \frac{1}{T}\sum_{t=0}^{T-1} P_t(v \mid \Psi_0), \tag{2.31}$$

converges for a finite position state space.[5] When we speak of a limiting distribution of a QRW we are considering this average distribution.

2.3.3. APPLICATIONS OF QUANTUM RANDOM WALKS

Because of these different properties of a QRW, it has been used to speed up several existing classical algorithms. An example is the quantum PageRank algorithm, which outperforms the classical PageRank algorithm in the sense that it should reveal the topology of the network more univocally. [11] Another application where a QRW based algorithm performs better than a classical algorithm is a database search. A classical algorithm needs $O(N)$ steps to find a target element in a database of size N, whereas it has been shown that a QRW based algorithm can find the target element within $O(\sqrt{N})$ steps. [11] The application of the CRW to a cards shuffle algorithm is somewhat more difficult to translate to a QRW based algorithm. When shuffling cards the main goal is to reach a distribution of cards which is independent of the initial distribution which is difficult for QRW algorithms because of the unitary evolution.

3

THE QUANTUM RANDOM WALK ON A HARMONIC OSCILLATOR

3.1. THE QUANTUM HARMONIC OSCILLATOR

In classical mechanics, a harmonic oscillator is often represented by a mass m on a spring with force constant k. The mass experiences a force $F = -kx$ and the potential energy is $V = \frac{1}{2}kx^2$. This model is very useful since many oscillatory motions may be described by the harmonic oscillator when we consider small motion around a minimum. This is because if we expand a potential $V(x)$ around a minimum at x_0 using a Taylor Expansion, we get that for x close to x_0:

$$V(x) = V(x_0) + V'(x_0)(x - x_0) + \frac{1}{2}V''(x_0)(x - x_0)^2 + \dots \tag{3.1}$$

Since x_0 is a minimum we have that $V'(x_0) = 0$ and we can substract the constant $V(x_0)$ without affecting the force, we get that

$$V(x) \approx \frac{1}{2}V''(x_0)(x - x_0)^2, \tag{3.2}$$

which describes a small harmonic oscillation around x_0.

In quantum mechanics an analogous model is often used to approximate the motion of a particle near equilibrium (thus near a minimum of $V(x)$). We call this model the Quantum Harmonic Oscillator [8], in which we are looking for solutions to the Schrödinger equation from Equation (2.8) with a harmonic potential

$$V(x) = \frac{1}{2}m\omega^2 x^2, \tag{3.3}$$

where $\omega \equiv \sqrt{\frac{k}{m}}$ describes the angular frequency of the oscillation.

We may then write the time-independent Schrödinger equation in the form

$$H\psi = \frac{1}{2m}\left[\hat{p}^2 + \left(m\omega\hat{x}\right)^2\right]\psi = E\psi, \tag{3.4}$$

where $\hat{p} \equiv (\frac{\hbar}{i}\frac{d}{dx})$ and $\hat{x}$ are the momentum and position operators respectively.

We introduce the following *ladder operators*

$$\hat{a}^\dagger \equiv \frac{1}{\sqrt{2\hbar m\omega}}(-i\hat{p} + m\omega\hat{x}) \tag{3.5a}$$

$$\hat{a} \equiv \frac{1}{\sqrt{2\hbar m\omega}}(i\hat{p} + m\omega\hat{x}) \tag{3.5b}$$

which we can use to rewrite the Schrödinger equation from Equation (3.4) as

$$\hbar\omega\left(\hat{a}\hat{a}^\dagger - \frac{1}{2}\right)\psi = E\psi, \text{ or} \tag{3.6a}$$

$$\hbar\omega\left(\hat{a}^\dagger\hat{a} + \frac{1}{2}\right)\psi = E\psi. \tag{3.6b}$$

From this we can see that if ψ is a solution to the Schrödinger equation with energy E, then $\hat{a}^\dagger\psi$ is a solution to the Schrödinger equation with energy $E + \hbar\omega$. Also, $\hat{a}\psi$ is a solution to the Schrödinger equation with energy $E - \hbar\omega$. This is why $\hat{a}^\dagger$ and $\hat{a}$ are called ladder operators for which $\hat{a}^\dagger$ is the *raising operator* or *creation operator* and $\hat{a}$ is the *lowering operator* or *annihilation operator*.

Since there should be a lowest energy, a lowest energy eigenstate of the system ψ_0 should exist for which we have that

$$\hat{a}\psi_0 = \frac{1}{\sqrt{2\hbar m\omega}}\left(i\frac{\hbar}{i}\frac{d\psi_0}{dx} + m\omega x\psi_0\right) = 0. \tag{3.7}$$

Thus

$$\frac{d\psi_0}{dx} = -\frac{m\omega}{\hbar}x\psi_0 \tag{3.8}$$

which is solved by

$$\psi_0(x) = A_0 e^{-\frac{m\omega}{2\hbar}x^2}, \tag{3.9}$$

where A_0 is a normalization constant such that $\int |\psi_0|^2 dx = 1$.

We can now find the energy of the lowest state by plugging Equation (3.9) into our Schrödinger equation in the form of Equation (3.6b), from which we can see that since $\hat{a}\psi_0 = 0$ we have that

$$E_0 = \frac{1}{2}\hbar\omega. \tag{3.10}$$

The energy eigenstate of the harmonic oscillator that is associated with E_0 is denoted as $|n = 0\rangle = |0\rangle$.

Now we can find the wave function of the excited states by applying the raising operator to $\psi_0(x)$, from which it follows that for discrete (quantized) levels $n \in \mathbb{N}$ the wave function and energy level for each possible excitation of the harmonic oscillator are given by

$$\psi_n(x) = A_n(\hat{a}^\dagger)^n e^{-\frac{m\omega}{2\hbar}x^2} \tag{3.11a}$$

$$E_n = (n + \frac{1}{2})\hbar\omega, \tag{3.11b}$$

where A_n is again a normalization constant such that $\int |\psi_n|^2 dx = 1$. The eigenenergies of the harmonic oscillator are equally spaced with a difference of $\hbar\omega$, which corresponds to the energy of one photon of frequency ω. The energy eigenstates of the harmonic oscillator that are associated with E_n are denoted as $|n\rangle$. The states $\{|n\rangle, n \in \mathbb{N}\}$ are called the *Fock states* and are labeled by the photon occupation number of the state. The Fock states form an orthonormal basis. Applying the creation or annihilation operators to a Fock state yields the transformations:

$$\begin{aligned} \hat{a}^\dagger |n\rangle &= \sqrt{n+1}\,|n+1\rangle, \\ \hat{a}\,|n\rangle &= \sqrt{n}\,|n-1\rangle, \\ \hat{a}^\dagger \hat{a}\,|n\rangle &= n\,|n\rangle. \end{aligned} \tag{3.12}$$

The operator $\hat{a}^\dagger \hat{a}$ is therefore also called the *number operator*.

A system that behaves as a quantum harmonic oscillator can be coupled to a spin-$\frac{1}{2}$ particle which makes it possible to perform a discrete QRW on such a system, which we will explore further in this chapter.

3.2. THE JAYNES-CUMMINGS HAMILTONIAN

We now consider a two-level atom with a ground state $|g\rangle$ and an excited state $|e\rangle$, interacting with a single-mode optical cavity field.

3.2.1. QUANTIZATION OF THE ELECTROMAGNETIC FIELD

The single-mode cavity field can be quantized in a way analogous to the quantization of the harmonic oscillator shown before. [12]

The energy of a single-mode EM-field (and thus the Hamiltonian H) is given by the following integral

$$H = \frac{1}{2}\int \left[\epsilon_0 \mathbf{E}^2(\mathbf{r}, t) + \frac{1}{\mu_0}\mathbf{B}^2(\mathbf{r}, t)\right] dV. \tag{3.13}$$

This looks very similar to the Hamiltonian of a harmonic oscillator from Equation (3.4). In fact, we may write the expressions for the electric and magnetic field such that intuitively they take the role of the position and momentum operator with mass $m = 1$ as seen in the previous section about the quantum harmonic oscillator. We use the ladder operators to express a field that satisfies Maxwell's equations in a one-dimensional

cavity along the z-axis with perfectly conducting walls at $z = 0, z = L$ as

$$\mathbf{E} = \mathbf{e}_x \left(\frac{\hbar\omega}{\epsilon_0 V}\right)^{\frac{1}{2}} (\hat{a}_k + \hat{a}_k^\dagger) \sin kz, \tag{3.14a}$$

$$\mathbf{B} = \mathbf{e}_y \left(\frac{\mu_0\epsilon_0}{k}\right)\left(\frac{\hbar\omega}{\epsilon_0 V}\right)^{\frac{1}{2}} (\hat{a}_k - \hat{a}_k^\dagger) \cos kz, \tag{3.14b}$$

where $\mathbf{e}_x$ and $\mathbf{e}_y$ are polarization vectors, $k = \frac{\omega}{c}$ is the wave number, V, is the effective volume of the cavity and ϵ_0 and μ_0 are the vacuum permittivity and permeability constant respectively. To satisfy the boundary conditions, the allowed frequencies of the field are of the form $\omega_m = \frac{cm\pi}{L}$ with $m \in \mathbb{N}$.

If we choose a value for k such that we are considering a single mode of the EM-field, we can calculate the Hamiltonian of this single mode using Equation (3.13), which gives:

$$\hat{H}_{\text{field}} = \hbar\omega\left(\hat{a}^\dagger \hat{a} + \frac{1}{2}\right), \tag{3.15}$$

which we recognize from the eigenenergies of the quantum harmonic oscillator in Equation (3.11b).

3.2.2. THE JAYNES-CUMMINGS MODEL

We have now quantized the cavity field. The total Hamiltonian of the two-level atom and cavity together will be of the form

$$\hat{H} = \hat{H}^{(0)}_{\text{atom}} + \hat{H}^{(0)}_{\text{field}} + \hat{H}^{(1)}, \tag{3.16}$$

where $\hat{H}^{(0)}_{\text{atom}}$ is the free atomic Hamiltonian, $\hat{H}^{(0)}_{\text{field}}$ is the free-field Hamiltonian and $\hat{H}^{(1)}$ is the interaction Hamiltonian between the atom and the field.

For convenience we define the energy level of the excited state $|e\rangle$ of the atom as $E_e = \frac{1}{2}\hbar\omega_0$ and the energy level of the ground state $|g\rangle$ as $E_g = -\frac{1}{2}\hbar\omega_0$ such that the energy difference between $|e\rangle$ and $|g\rangle$ is equal to $\hbar\omega_0$. We now introduce atomic transition operators that are similar to the ladder operators we saw in the Quantum Harmonic Oscillator model.

$$\hat{\sigma}_+ = |e\rangle\langle g| \tag{3.17a}$$

$$\hat{\sigma}_- = |g\rangle\langle e| \tag{3.17b}$$

$$\hat{\sigma}_z = |e\rangle\langle e| - |g\rangle\langle g| \tag{3.17c}$$

It follows that the Hamiltonian of the two-level atom is given by

$$\hat{H}^{(0)}_{\text{atom}} = \frac{1}{2}\hbar\omega_0\hat{\sigma}_z. \tag{3.18}$$

The interaction between the cavity field and the two-level atom is often given by a dipole coupling

$$\hat{H}^{(1)} = -\hat{\mathbf{d}}\cdot\hat{\mathbf{E}}, \tag{3.19}$$

We can write $\hat{H}^{(1)}$ as

$$-\hat{\mathbf{d}}\cdot\hat{\mathbf{E}} = \hat{d}g\left(\hat{a}+\hat{a}^\dagger\right) \tag{3.20}$$

with

$$g = -\left(\frac{\hbar\omega}{\epsilon_0 V}\right)^{1/2}\sin kz, \tag{3.21a}$$

$$\hat{d} = \hat{\mathbf{d}}\cdot\mathbf{e}. \tag{3.21b}$$

The dipole operator $\hat{d}$ is an odd operator and therefore all diagonal elements of the corresponding transition matrix are zero. We may then write $\hat{d}$ in terms of its off-diagonal elements as follows: $\hat{d} = d\left|g\right\rangle\langle e| + d^*\left|e\right\rangle\langle g| = d\hat{\sigma}_- + d^*\hat{\sigma}_+ = d(\hat{\sigma}_+ + \hat{\sigma}_-)$, where we may assume that d is real for simplicity.

Therefore we may write the interaction Hamiltonian as

$$\hat{H}^{(\mathrm{I})} = \hbar\lambda\,(\hat{\sigma}_+ + \hat{\sigma}_-)\left(\hat{a}+\hat{a}^\dagger\right) \tag{3.22}$$

where $\lambda = dg/\hbar$.

From this expression four terms arise: $\hat{\sigma}_+\hat{a}$, $\hat{\sigma}_-\hat{a}^\dagger$, $\hat{\sigma}_+\hat{a}^\dagger$, $\hat{\sigma}_-\hat{a}$. The time dependent expression for each of the terms can be derived from Heisenberg's equation using the free field Hamiltonians of the field and the atom. Since the operators $\hat{a}$ and $\hat{\sigma}_\pm$ have no explicit time dependence, Heisenberg's equation for each of the individual operators is given by

$$\frac{d}{dt}\hat{a}^\dagger(t) = \frac{i}{\hbar}\left[\hbar\omega(\hat{a}^\dagger\hat{a}+\frac{1}{2}),\hat{a}^\dagger\right] = i\omega\hat{a}^\dagger, \tag{3.23a}$$

$$\frac{d}{dt}\hat{a}(t) = \frac{i}{\hbar}\left[\hbar\omega(\hat{a}^\dagger\hat{a}+\frac{1}{2}),\hat{a}\right] = -i\omega\hat{a}, \tag{3.23b}$$

$$\frac{d}{dt}\hat{\sigma}_\pm(t) = \frac{i}{\hbar}\left[\frac{1}{2}\hbar\omega_0\sigma_z,\hat{\sigma_\pm}\right] = \pm\sigma_\pm\omega_0. \tag{3.23c}$$

It follows that $\hat{a}^\dagger(t) = \hat{a}^\dagger(0)e^{i\omega t}$, $\hat{a}(t) = \hat{a}(0)e^{-i\omega t}$, $\sigma_\pm(t) = \sigma_\pm(0)e^{\pm i\omega_0 t}$. The time dependent terms in Equation (3.22) then evolve proportional to

$$\begin{aligned}\hat{\sigma}_+\hat{a} &\sim e^{i(\omega_0-\omega)t},\\ \hat{\sigma}_-\hat{a}^\dagger &\sim e^{i(\omega-\omega_0)t},\\ \hat{\sigma}_+\hat{a}^\dagger &\sim e^{i(\omega_0+\omega)t},\\ \hat{\sigma}_-\hat{a} &\sim e^{-i(\omega_0+\omega)t},\end{aligned} \tag{3.24}$$

where we can see that the last two terms are much more rapidly oscillating terms than the first two, when considering frequencies of the field such that $\omega \approx \omega_0$. Here we make a *Rotating Wave Approximation*, where we neglect the fast oscillating terms with a frequency $(\omega+\omega_0)$ since they will average to zero.

Intuitively this makes sense because the term $\hat{\sigma}_+\hat{a}^\dagger$ corresponds to a transition where the atom moves to the excited state while a photon is created simultaneously, and the term

$\hat{\sigma}_- \hat{a}$ corresponds to the atom moving to the ground state while a photon is annihilated. These are events that are not as likely to occur as the other two transitions. Therefore we may approximate the interaction Hamiltonian as follows:

$$\hat{H}^{(1)} = \hbar\lambda\left(\hat{\sigma}_+ \hat{a} + \hat{\sigma}_- \hat{a}^\dagger\right). \tag{3.25}$$

and we have a total Hamiltonian given by

$$\hat{H} = \frac{1}{2}\hbar\omega_0 \hat{\sigma}_z + \hbar\omega \hat{a}^\dagger \hat{a} + \hbar\lambda\left(\hat{\sigma}_+ \hat{a} + \hat{\sigma}_- \hat{a}^\dagger\right). \tag{3.26}$$

Here we have dropped the term $\hbar\omega/2$ from the free-field Hamiltonian for convenience, which is allowed because of the choice for a zero-point energy.

This Hamiltonian is called the *Jaynes-Cummings Hamiltonian*. [12] We may write this in a simpler form as follows

$$\hat{H} = \hbar\omega\hat{N} + \hbar\delta\hat{\sigma}_z + \hbar\lambda\left(\hat{\sigma}_+ \hat{a} + \hat{\sigma}_- \hat{a}^\dagger\right), \tag{3.27}$$

where $N = \hat{a}^\dagger \hat{a} + \frac{\hat{\sigma_z}}{2}$ and the detuning between the cavity field and the atom $\delta = \frac{\omega_0 - \omega}{2}$. The constant $\hbar$ is often set to 1 for convenience.

For $\omega = \delta = 0$ we can see that

$$\begin{aligned} H\frac{1}{\sqrt{2}}[|n,e\rangle + |n+1,g\rangle] &= \lambda\left(\hat{\sigma}_+ \hat{a} + \hat{\sigma}_- \hat{a}^\dagger\right)\frac{1}{\sqrt{2}}[|n,e\rangle + |n+1,g\rangle] \\ &= \lambda\frac{1}{\sqrt{2}}[\sqrt{n+1}\,|n+1,e\rangle + \sqrt{n+1}\,|n,g\rangle], \end{aligned} \tag{3.28a}$$

$$\begin{aligned} H\frac{1}{\sqrt{2}}[|n,e\rangle - |n+1,g\rangle] &= \lambda\left(\hat{\sigma}_+ \hat{a} + \hat{\sigma}_- \hat{a}^\dagger\right)\frac{1}{\sqrt{2}}[|n,e\rangle - |n+1,g\rangle] \\ &= \lambda\frac{1}{\sqrt{2}}[\sqrt{n+1}\,|n+1,e\rangle - \sqrt{n+1}\,|n,g\rangle]. \end{aligned} \tag{3.28b}$$

Thus $|\chi_n\rangle = \frac{1}{\sqrt{2}}[|n,e\rangle + |n+1,g\rangle]$ is an eigenstate of H with eigenvalue $\lambda\sqrt{n+1}$, and $|\overline{\chi_n}\rangle = \frac{1}{\sqrt{2}}[|n,e\rangle - |n+1,g\rangle]$ is an eigenstate of H with eigenvalue $-\lambda\sqrt{n+1}$. The values of the ket are labeled |field, atom⟩. [9]

RABI OSCILLATIONS

We will now look at the the Hamiltonian for the subspace spanned by the states $|0,0\rangle, |0,1\rangle, |1,0\rangle$. The values are again labeled |field, atom⟩, where we define $|.,0\rangle = |.,g\rangle$ and $|.,1\rangle = |.,e\rangle$. Note that with this convention, for this section the Pauli-z operator in the subspace spanned by $|n,0\rangle, |n,1\rangle$ is defined as

$$\hat{\sigma}_z = \begin{bmatrix} -1 & 0 \\ 0 & 1 \end{bmatrix}. \tag{3.29}$$

We may neglect the term $\hat{N}$ from Equation (3.26) because we may enter a *rotating frame* by applying the unitary transformation $U = e^{i\omega\hat{N}t}$ to obtain an interaction Hamiltonian $H_{\text{int}} = UHU^\dagger + i\hbar\dot{U}U^\dagger$.

We find that we can write the interaction Hamiltonian in matrix form as:

$$H_{\text{int}} = \begin{bmatrix} -\delta & 0 & 0 \\ 0 & \delta & \lambda \\ 0 & \lambda & -\delta \end{bmatrix} \tag{3.30}$$

where the basis states from left to right and from top to bottom are $|0,0\rangle, |0,1\rangle, |1,0\rangle$.

This follows from the fact that the term $\delta\hat{\sigma}_z$ only contributes on diagonal elements and we have by Equation (3.17c) that $\delta\hat{\sigma}_z|0,0\rangle = -\delta|0,0\rangle, \delta\hat{\sigma}_z|0,1\rangle = \delta|0,1\rangle$, and $\delta\hat{\sigma}_z|1,0\rangle = -\delta|1,0\rangle$. The term $\lambda\left(\hat{\sigma}_+\hat{a} + \hat{\sigma}_-\hat{a}^\dagger\right)$ gives the off-diagonal elements since $\lambda\left(\hat{\sigma}_+\hat{a} + \hat{\sigma}_-\hat{a}^\dagger\right)|0,1\rangle = \lambda|1,0\rangle$ and $\lambda\left(\hat{\sigma}_+\hat{a} + \hat{\sigma}_-\hat{a}^\dagger\right)|1,0\rangle = \lambda|0,1\rangle$.

We now look at the interaction Hamiltonian of the subspace spanned by the states $|0,1\rangle, |1,0\rangle$:

$$H_{\text{int}} = \begin{bmatrix} \delta & \lambda \\ \lambda & -\delta \end{bmatrix} = \lambda\hat{\sigma}_x + \delta\hat{\sigma}_z \tag{3.31}$$

and use the fact that we can write e^{-iHt} as $e^{i\mathbf{n}\cdot\boldsymbol{\sigma}}$ where $\mathbf{n} = -t(\lambda, 0, \delta)$ and $\boldsymbol{\sigma} = (\hat{\sigma}_x, \hat{\sigma}_y, \hat{\sigma}_z)$ and we use that

$$e^{i\mathbf{n}\cdot\boldsymbol{\sigma}} = \cos|\mathbf{n}| \cdot I + i\hat{\boldsymbol{n}}\cdot\boldsymbol{\sigma}\sin|\mathbf{n}|, \tag{3.32}$$

where $\hat{\mathbf{n}}$ is the unit vector of $\mathbf{n}$.

It follows that the unitary operator corresponding to evolution of Equation (3.31) is equal to

$$\begin{bmatrix} \cos\Omega t - \frac{i\delta}{\Omega}\sin\Omega t & -\frac{i\lambda}{\Omega}\sin\Omega t \\ -\frac{i\lambda}{\Omega}\sin\Omega t & \cos\Omega t + \frac{i\delta}{\Omega}\sin\Omega t \end{bmatrix}, \tag{3.33}$$

with $\Omega = \sqrt{\lambda^2 + \delta^2}$

Together with the Hamiltonian for $|0,0\rangle$ we get that we can write the total time dependent unitary operator $U = e^{-iHt}$ as

$$\begin{aligned} U = e^{i\delta t}|0,0\rangle\langle 0,0| \\ +(\cos\Omega t - \frac{i\delta}{\Omega}\sin\Omega t)|0,1\rangle\langle 0,1| \\ +\cos\Omega t + \frac{i\delta}{\Omega}\sin\Omega t|1,0\rangle\langle 1,0| \\ -\frac{i\lambda}{\Omega}\sin\Omega t(|0,1\rangle\langle 1,0| + |1,0\rangle\langle 0,1|). \end{aligned} \tag{3.34}$$

Here we see in the last term of Equation (3.34) that an oscillation at a frequency Ω occurs where the field and the atom exchange a photon. These oscillations are called *Rabi oscillations* and Ω is called the *Rabi frequency*. In comparison to the classic case we see that

these oscillations even arise when the field is in the so-called *vacuum state*, i.e. $n = 0$. This is the result of an atom spontaneously emitting a photon and re-absorbing and re-emitting it. [9]

If we extend the calculation we did above to the Hamiltonian of the subspace spanned by the states $|n,1\rangle$ and $|n+1,0\rangle$, we find the following matrix notation of the Hamiltonian:

$$H = \begin{bmatrix} \delta & \lambda\sqrt{n+1} \\ \lambda\sqrt{n+1} & -\delta \end{bmatrix} = \lambda\sqrt{n+1}\hat{\sigma}_x + \delta\hat{\sigma}_z \tag{3.35}$$

We can write e^{-iHt} as $e^{i\mathbf{n}\cdot\boldsymbol{\sigma}}$ where $\mathbf{n} = -t(\lambda\sqrt{n+1}, 0, \delta)$ and $\boldsymbol{\sigma} = (\sigma_x, \sigma_y, \sigma_z)$. It then follows from Equation (3.32) that we can write the total time dependent unitary operator of this subspace as

$$\begin{aligned} U = &\begin{bmatrix} \cos\Omega t - \frac{i\delta}{\Omega_n}\sin\Omega_n t & -\frac{i\lambda\sqrt{n+1}}{\Omega_n}\sin\Omega_n t \\ -\frac{i\lambda\sqrt{n+1}}{\Omega_n}\sin\Omega_n t & \cos\Omega_n t + \frac{i\delta}{\Omega_n}\sin\Omega_n t \end{bmatrix} \\ =&(\cos\Omega_n t - \frac{i\delta}{\Omega_n}\sin\Omega_n t)\,|n,1\rangle\langle n,1| \\ &+ (\cos\Omega_n t + \frac{i\delta}{\Omega_n}\sin\Omega_n t)\,|n+1,0\rangle\langle n+1,0| \\ &- \frac{i\lambda\sqrt{n+1}}{\Omega_n}\sin\Omega_n t(|n,1\rangle\langle n+1,0| + |n+1,0\rangle\langle n,1|) \end{aligned} \tag{3.36}$$

where $\Omega_n = \sqrt{\lambda^2(n+1)+\delta^2}$. We see that when the detuning $\delta = 0$, the Rabi oscillations between states $|n,1\rangle, |n+1,0\rangle$ oscillate $\sqrt{n+1}$ times faster than the vacuum Rabi oscillations for $n = 0$.

DISPERSIVE REGIME OF THE JAYNES-CUMMINGS MODEL

We have now studied the behaviour of the Jaynes-Cummings model in the near-resonant regime ($\omega_0 \approx \omega, \delta = 0$), but the Jaynes-Cummings Hamiltonian takes an interesting form in the case of large detuning. If we detune the field such that δ is much larger than the coupling strength λ, in the limit $\frac{\lambda}{\delta^2} \ll 1$ which we call the *dispersive limit* we may the Hamiltonian by a perturbative expansion as follows:

$$H_{\text{eff}} = (\omega + \chi\sigma_z)\hat{a}^\dagger\hat{a} + \frac{1}{2}(\omega_0 + \chi)\sigma_z, \tag{3.37}$$

with $\chi = \frac{\lambda^2}{\delta}$. This perturbative expansion holds for a photon number below the critical photon number $n_{\text{crit}} = \frac{\delta^2}{4\lambda^2}$. [13]

3.3. PHYSICAL IMPLEMENTATIONS OF THE QRW

In this research we will focus on an implementation of the QRW with superconducting qubits in circuit-QED. [3]The QRW has been implemented in several other physical systems in previous research such as Trapped Ions, which we will shortly describe as well.

3.3.1. TRAPPED IONS

The setup of trapped ions is achieved by trapping ions such as $^9Be^+$ in between electrodes with a radiofrequency potential that creates an electromagnetic field. The spin states of a single valence electron of the ion represent a qubit in trapped ion quantum computers. These spin states are used as coin states of the QRW and the position of the ion in the trap gives the motional degree of freedom for the QRW. A sequence of Raman beam pulses is used to change the state of the qubit and to displace the position of the ion such that the conditional displacement of the QRW can be performed. A QRW setup for the walk on a line and circle using trapped ions have been researched. [14]

3.3.2. CAVITY AND CIRCUIT QUANTUM ELECTRODYNAMICS

Optical cavity quantum electrodynamics and circuit quantum electrodynamics (QED) are two closely related fields that have shown promising applications for physical setups for a quantum computer. Both are based on the interaction between light and matter by coupling. The interaction between photons in a single mode electromagnetic field in a superconducting cavity and a two-level atom have been studied in Section 3.2.2. In circuit quantum electrodynamics (QED) [3] the cavity may also be replaced by an LC resonator on a chip and the two-level atom is replaced by an artificial atom such as a transmon qubit. The transmon qubit is an artificial atom that is created by replacing the inductance in an LC resonator by a Josephson junction to create anharmonicity. The quantized energy levels of the transmon qubit are not equidistant, which is necessary to be able to address only the ground state and first excited state. The lower two levels of the transmon qubit may now be used as the two states of a qubit. The transmon qubit can now be capacitively coupled to the resonator. The Hamiltonian of this combined system is the Jaynes-Cummings Hamiltonian we studied in Section 3.2.2.

QRW's in circles in phase space have been implented using superconducting circuit-QED. [15] A 2D QRW has recently been implemented on a 62-bit superconducting quantum computer on multiple oscillators. [16]

3.4. IMPLEMENTATION OF THE QRW ON THE FOCK STATES OF A HARMONIC OSCILLATOR

We will now look at the implementation of the QRW on a system consisting of a two-level particle coupled to an oscillator.

In Chapter 2 we have seen how the evaluation of the discrete QRW on an infinite 1D line is described. This was done by performing a shift operation and a coin flip operation for each step of the walk. We explore using the transformation that occurs because of the Rabi oscillations we studied in Section 3.2.2, followed by flipping the state of the two level atom, to perform the conditional shift of the QRW.

To do this, we want to set the variables of the system such that the Jaynes-Cummings

Hamiltonian operator results in the following transformation:

$$\begin{aligned} |n,1\rangle &\longleftrightarrow |n+1,0\rangle \quad n \geq 0, \\ |0,0\rangle &\longleftrightarrow |0,0\rangle . \end{aligned} \tag{3.38}$$

Recall from Section 2.3.1 that in the Discrete QRW we want a conditional shift:

$$|n,1\rangle \xrightarrow{S} |n+1,1\rangle , \tag{3.39a}$$

$$|n+1,0\rangle \xrightarrow{S} |n,0\rangle , \tag{3.39b}$$

where n is the number of photons and $0,1$ corresponds to the state of the qubit. Note that in this section the directions of the walk corresponding to each coin state are opposite from the definitions in Chapter 2 and in Chapter 4.

We can achieve the same shift if we first perform an operator that transforms the state of the system as in Equation (3.38) and then use the operator $\hat{\sigma}_x$ which is a flip of the two-level atom state. We now have that

$$|n,1\rangle \xrightarrow{Equation\ (3.38)} |n+1,0\rangle \xrightarrow{\hat{\sigma}_x} |n+1,1\rangle , \tag{3.40a}$$

$$|n+1,0\rangle \xrightarrow{Equation\ (3.38)} |n,1\rangle \xrightarrow{\hat{\sigma}_x} |n,0\rangle , \tag{3.40b}$$

for $n \geq 0$, which is indeed equivalent to the conditional shift in position that we saw in the Discrete QRW on a 1D line. However, we now have to consider the boundary induced by the ground state $|0\rangle$ of the harmonic oscillator. For the state $|0,0\rangle$ the evolution of Equation (3.38) followed by $\hat{\sigma}_x$ creates the following state:

$$|0,0\rangle \xrightarrow{Equation\ (3.38)} |0,0\rangle \xrightarrow{\hat{\sigma}_x} |0,1\rangle . \tag{3.41}$$

ADJUSTING THE FIELD TO IMPLEMENT THE QUANTUM RANDOM WALK ON THE HARMONIC OSCILLATOR

We now want to find how we can adjust the parameters of the unitary Jaynes-Cummings Hamiltonian operator so that the operator transforms the state of the system as in Equation (3.38). In order to do this we should adjust the frequency of the oscillator such that the oscillator and qubit couple with zero detuning $\delta = 0$ for the correct amount of time such that the Rabi frequence induces the right transition between each of the Fock states used in the walk. However, one problem with this idea is that the Rabi frequency Ω_n is different for different levels of the quantum walks since it is dependent on n, which makes this setup a difficult way to implement the QRW. In the next chapter we will consider a setup of a QRW that does not use the different Fock states of an oscillator as its position state space, but rather walks in phase space between coherent states. We will shortly study what the effect of a boundary at $|0\rangle$ is on a QRW that evolves as Equation (3.40) and Equation (3.41).

QUANTUM RANDOM WALK ON HARMONIC OSCILLATOR FOCK STATES WITH BOUNDARY

A difference from the walk on the 1D infinite line is that a quantum harmonic oscillator has a ground state which is a lower boundary to the field states. This means that the allowed position states of the walk (corresponding to the modes of the field) are $\{|n\rangle : n \in \mathbb{N}\}$ instead of $n \in \mathbb{Z}$. For the probability distribution of the QRW this would imply a reflective or Neumann boundary at the vacuum Fock state $|0\rangle$. We shortly study the effect of this boundary in a numerical simulation, before moving on to the implementation of the QRW in a different and more realizable setup.

A unitary operator that realises the evolution of the walk from Equation (3.40) and Equation (3.41) is given by

$$U = H \cdot \hat{\sigma}_x \cdot W, \tag{3.42}$$

where

$$W = \begin{bmatrix} 1 & 0 & 0 & \dots & \dots & \cdots = & 0 \\ 0 & \begin{bmatrix} 0 & 1 \\ 1 & 0 \end{bmatrix} & & & & & \vdots \\ 0 & & & & & & \vdots \\ \vdots & & & \ddots & & & \vdots \\ \vdots & & & & \begin{bmatrix} 0 & 1 \\ 1 & 0 \end{bmatrix} & & 0 \\ \vdots & & & & & & 0 \\ 0 & \dots & \dots & \dots & 0 & 0 & 1 \end{bmatrix} \tag{3.43}$$

$$\hat{\sigma}_x = \begin{bmatrix} \begin{bmatrix} 0 & 1 \\ 1 & 0 \end{bmatrix} & 0 & \dots & 0 & 0 \\ 0 & 0 & \ddots & & \vdots & \vdots \\ \vdots & \vdots & & \ddots & 0 & 0 \\ 0 & & \dots & 0 & \begin{bmatrix} 0 & 1 \\ 1 & 0 \end{bmatrix} & \\ 0 & 0 & \dots & 0 & & \end{bmatrix}, \tag{3.44}$$

and

$$H = \frac{1}{\sqrt{2}} \begin{bmatrix} \begin{bmatrix} 1 & 1 \\ 1 & -1 \end{bmatrix} & 0 & \dots & 0 & 0 \\ 0 & 0 & \ddots & & \vdots & \vdots \\ \vdots & \vdots & & \ddots & 0 & 0 \\ 0 & & \dots & 0 & \begin{bmatrix} 1 & 1 \\ 1 & -1 \end{bmatrix} & \\ 0 & 0 & \dots & 0 & & \end{bmatrix}. \tag{3.45}$$

Theoretically, a harmonic oscillator does not have an upper bound state. To implement this effect in numerical simulations of the QRW on the Fock states of a harmonic oscillator we choose a position space for the walk that is always large enough for the number of steps t that will be performed, such that the walk does go beyond the upper boundary

of the numerical position space. This can be done by creating a position Hilbert space spanned by the states $\{|0\rangle, ..., |x_0 + t\rangle\}$ for a walk that starts in initial position state $|x_0\rangle$. This is why the matrix W has a 1 in the bottom right corner such that W is unitary. It does not affect the evolution of the walk since the walk will only reach the upper bound state at the last step.

The probability distribution for the initial states $|\Psi_0\rangle = |50\rangle \otimes (|0\rangle + i\,|1\rangle)/\sqrt{2}$ and $|\Psi_0\rangle = |0\rangle \otimes (|0\rangle + i\,|1\rangle)/\sqrt{2}$ are plotted in Figure 3.1 and Figure 3.2 respectively.

From these figures it seems that the peaks that are travelling to the left are reflected back to the right. Indeed if we plot the indices of the position of the 2 peaks (i.e. the maxima of the probability distribution of the QRW) against the number of steps, this reflection is clearly visible in Figure 3.3 and Figure 3.4.

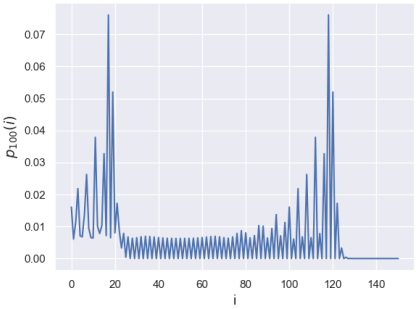

Figure 3.1: Probability distribution of the one-dimensional QRW with a boundary at 0, after 100 steps and initial state $|50\rangle \otimes (|0\rangle + i\,|1\rangle)/\sqrt{2}$

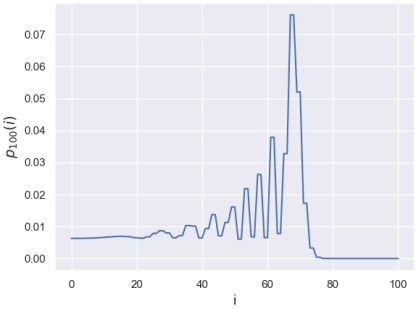

Figure 3.2: Probability distribution of the one-dimensional QRW with a boundary at 0, after 100 steps and initial state $|0\rangle \otimes (|0\rangle + i\,|1\rangle)/\sqrt{2}$

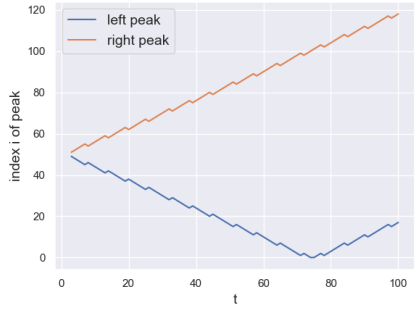

Figure 3.3: Index of the two maxima of a QRW with a boundary at 0 and initial state $|50\rangle \otimes (|0\rangle + i\,|1\rangle)/\sqrt{2}$, plotted against number of steps t.

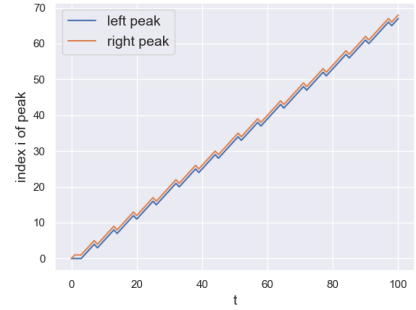

Figure 3.4: Index of the two maxima of a QRW with a boundary at 0 and initial state $|0\rangle \otimes (|0\rangle + i\,|1\rangle)/\sqrt{2}$, plotted against number of steps t.

4

IMPLEMENTATION OF THE QUANTUM RANDOM WALK ON SUPERCONDUCTING CIRCUIT-QED IN PHASE SPACE

In the previous chapter an overview of the physical setups to realise a QRW were given and the implementation of a QRW on the Fock States of a quantum harmonic oscillator was investigated. In this chapter, coherent states and displacements are introduced as a tool for performing the QRW on the 2D grid in phase space in superconducting circuit-QED. Results of a walk on the 2D grid in phase space are examined.

4.1. THE DISPLACEMENT OPERATOR AND COHERENT STATES

In the previous chapter we explored Fock states of the quantum harmonic oscillator. We will now look at a different type of states associated with the harmonic oscillator, called *coherent states*. [13] The coherent states are described by a complex amplitude α. Intuitively this α represents the amplitude and phase by which the oscillator is displaced. The coherent states are induced by a unitary operator we call the *displacement operator*. It is defined as follows:

$$D(\alpha) = e^{\alpha \hat{a}^\dagger - \alpha^* \hat{a}}. \tag{4.1}$$

A coherent state $|\alpha\rangle$ is defined as $D(\alpha)|0\rangle$, where $|0\rangle$ is the vacuum state which corresponds to a zero displacement of the oscillator.

We can write $D(\alpha)D(\beta) = e^A e^B$ with $A = \alpha\hat{a}^\dagger - \alpha^*\hat{a}$ and $B = \beta\hat{a}^\dagger - \beta^*\hat{a}$. The Baker-

Campbell-Hausdorf lemma gives the solution for Z to the equation $e^X e^Y = e^Z$:

$$Z = X + Y + \frac{1}{2}[X,Y] + \frac{1}{12}[X,[X,Y]] - \frac{1}{12}[Y,[X,Y]] + \cdots \tag{4.2}$$

Using $[\hat{a},\hat{a}^\dagger] = I$, we find that $[A,B] = \alpha\beta^* - \alpha^*\beta$. We then know that A and B both commute with $[A,B]$ and therefore the higher order terms of Equation (4.2) are equal to zero. Thus

$$\begin{aligned} D(\alpha)D(\beta) = e^A e^B = e^{(\alpha\hat{a}^\dagger - \alpha^*\hat{a}) + (\beta\hat{a}^\dagger - \beta^*\hat{a}) + (\alpha\beta^* - \alpha^*\beta)/2} = \\ e^{((\alpha+\beta)\hat{a}^\dagger - (\alpha+\beta)^*\hat{a})} e^{(\alpha\beta^* - \alpha^*\beta)/2} = D(\alpha+\beta)e^{(\alpha\beta^* - \alpha^*\beta)/2}. \end{aligned} \tag{4.3}$$

This shows that we have to account for extra phase factors when performing a sequence of displacements.

The Baker-Campbell-Hausdorf lemma can also be used to rewrite the displacement operator $D(\alpha)$. From $[\alpha\hat{a}^\dagger, \alpha^*\hat{a}] = -|\alpha|^2$ it follows that

$$D(\alpha) = e^{-|\alpha|^2/2} e^{\alpha\hat{a}^\dagger} e^{-\alpha^*\hat{a}}. \tag{4.4}$$

If we expand the exponentials as a power series we find that

$$D(\alpha)|0\rangle = e^{-|\alpha|^2/2} \sum_{n=0}^{\infty} \frac{\alpha^n \hat{a}^{\dagger n}}{n!} \sum_{m=0}^{\infty} \frac{\alpha^{*m}\hat{a}^m}{m!} |0\rangle. \tag{4.5}$$

We know that $\hat{a}|0\rangle = |0\rangle$ and $\hat{a}^{\dagger n}|0\rangle = \sqrt{n!}|n\rangle$ and thus it follows that we can write the coherent state $|\alpha\rangle$ in terms of Fock states as

$$|\alpha\rangle = D(\alpha)|0\rangle = \sum_{n=0}^{\infty} c_n |n\rangle = e^{-|\alpha|^2/2} \sum_{n=0}^{\infty} \frac{\alpha^n}{\sqrt{n!}} |n\rangle. \tag{4.6}$$

From this form we can see that the probability distribution of the coherent state $|a\rangle$ over the Fock states, $p_\alpha(n) = |c_n|^2$ is a Poisson distribution:

$$p_\alpha(n) = e^{-|\alpha|^2} \frac{\alpha^{2n}}{n!} \tag{4.7}$$

with parameter $\lambda = |\alpha|^2$. By the properties of a Poisson distribution it then follows that the mean photon number $\overline{n} = |\alpha|^2$ and the standard deviation is $|\alpha| = \sqrt{\overline{n}}$.

Two coherent states are not exactly orthogonal; the inner product between two coherent states is given by

$$\langle\alpha|\beta\rangle = e^{-|\alpha|^2/2} e^{-|\beta|^2/2} \sum_{n=0}^{\infty} \frac{(\alpha^*\beta)^n}{n!} = e^{-|\alpha|^2/2} e^{-|\beta|^2/2} e^{\alpha^*\beta} \tag{4.8}$$

for which the modulus squared is equal to

$$|\langle\alpha|\beta\rangle|^2 = e^{-|\alpha-\beta|^2}. \tag{4.9}$$

When α and β have a large difference in amplitude we may approximate two coherent states as orthogonal. [13]

A displacement as in Equation (4.1) corresponds to an evolution by a Hamiltonian

$$H = a\hat{p} + b\hat{q}, \tag{4.10}$$

which physically corresponds to driving an oscillator by applying an electromagnetic field. It has been shown that driving an oscillator using displacement pulses is physically realizable considering coherence times in circuit-QED. [17] We will further discuss this in the Discussion in Chapter 5.

4.1.1. CONTROLLED DISPLACEMENTS BY ROTATIONS

Now that we have examined the properties of the displacement operator we study how we could use the displacement operator on coherent states of a cavity field to perform a step of the QRW. In the QRW we need a conditional shift that depends on the state of a qubit that is coupled to the cavity. This conditional shift can be realised in superconducting circuit-QED using a *controlled rotation*. [18] To perform a controlled rotation we use the dispersive regime Jaynes-Cummings Hamiltonian.

For the dispersive regime, the effective Hamiltonian after applying a unitary change of frame transformation to Equation (3.37) is given by $\hat{H}_{\text{eff}} = \chi \hat{a}^\dagger \hat{a} \hat{\sigma}_z$, because we can neglect the uncoupled evolution of the qubit and oscillator. The unitary operator $\hat{U} = e^{-i\hat{H}_{\text{eff}}t}$ applied to a coherent state $|\alpha\rangle$ of the cavity gives a rotation of the coherent state, dependent on the state of the coupled qubit:

$$\hat{U}|\alpha\rangle = e^{-it\chi\hat{a}^\dagger\hat{a}\hat{\sigma}_z} \sum_{n=0}^{\infty} e^{-|\alpha|^2/2} \frac{\alpha^n}{\sqrt{n!}} |n\rangle = \sum_{n=0}^{\infty} e^{-|\alpha|^2/2} \frac{\alpha^n}{\sqrt{n!}} e^{-it\chi\hat{\sigma}_z n} |n\rangle = \left| e^{-i\theta\hat{\sigma}_z} \alpha \right\rangle \tag{4.11}$$

with $\theta = t\chi$, such that

$$\hat{U}|\alpha, 0\rangle = \left| e^{-i\theta} \alpha \right\rangle, \tag{4.12a}$$

$$\hat{U}|\alpha, 1\rangle = \left| e^{i\theta} \alpha \right\rangle. \tag{4.12b}$$

If we choose t such that $\theta = t\chi = \frac{\pi}{2}$ then the states $|\alpha, 0\rangle$ and $|\alpha, 1\rangle$ are rotated in phase space by $\frac{\pi}{2}$ clockwise and counterclockwise respectively, such that the states are separated by π. If we then perform an unconditional displacement $D(-i\beta)$ (on both of the states) and we rotate the states in reverse direction back by $\frac{\pi}{2}$, the states are conditionally displaced by $D(\pm\beta)$. For a sketch of the movement of each state in phase space see Figure 4.1.

The rotation in reverse direction is realised by the sequence of gates

$$X e^{-i\theta\hat{a}^\dagger\hat{a}\hat{\sigma}_z} X = X \sum_{n=0}^{\infty} \frac{(-i\theta\hat{a}^\dagger\hat{a}\hat{\sigma}_z)^n}{n!} X = \sum_{n=0}^{\infty} \frac{(-i\theta\hat{a}^\dagger\hat{a}X\hat{\sigma}_z X)^n}{n!} = e^{i\theta\hat{a}^\dagger\hat{a}\hat{\sigma}_z}, \tag{4.13}$$

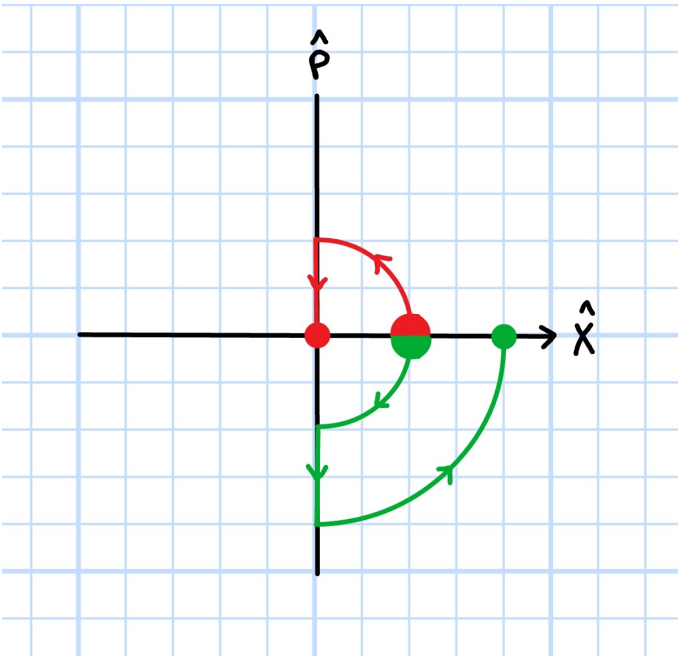

Figure 4.1: Sketch of the controlled displacement in phase space from $(|\alpha,0\rangle + |\alpha,1\rangle)/\sqrt{2}$ to the state $(|2\alpha,0\rangle + |0,1\rangle)/\sqrt{2}$, with $\alpha \in \mathbb{R}$. The green path corresponds to the $|0\rangle$ coin state and the red path corresponds to the $|1\rangle$ coin state.

where X is the Pauli-X gate.

Now we have that the total controlled displacement operator is given by $\tilde{D}(\beta) = R(\theta)^\dagger D(-i\beta)R(\theta)$, where $R(\theta) = e^{-i\theta\hat{a}^\dagger\hat{a}\hat{\sigma}_z}$ and $\theta = \frac{\pi}{2}$. Indeed this results in a controlled displacement of a state $|\alpha\rangle$ by $D(\beta\hat{\sigma}_z)$ for α and $\beta \in \mathbb{R}$, since

$$\begin{aligned} e^{i\frac{\pi}{2}\hat{a}^\dagger\hat{a}\hat{\sigma}_z} D(-i\beta) e^{-i\frac{\pi}{2}\hat{a}^\dagger\hat{a}\hat{\sigma}_z} |\alpha\rangle = e^{i\frac{\pi}{2}\hat{a}^\dagger\hat{a}\hat{\sigma}_z} D(-i\beta) \left|\alpha e^{-i\frac{\pi}{2}\hat{\sigma}_z}\right\rangle = \\ e^{i\frac{\pi}{2}\hat{a}^\dagger\hat{a}\hat{\sigma}_z} \left|\alpha e^{-i\frac{\pi}{2}\hat{\sigma}_z} - i\beta\right\rangle e^{(\alpha e^{-i\frac{\pi}{2}\hat{\sigma}_z} i\beta + \alpha e^{i\frac{\pi}{2}\hat{\sigma}_z} i\beta)/2} = \\ \left|e^{i\frac{\pi}{2}\hat{\sigma}_z}(\alpha e^{-i\frac{\pi}{2}\hat{\sigma}_z} - i\beta)\right\rangle e^{(\alpha e^{-i\frac{\pi}{2}\hat{\sigma}_z} i\beta + \alpha e^{i\frac{\pi}{2}\hat{\sigma}_z} i\beta)/2} = D(-i\beta e^{i\frac{\pi}{2}\hat{\sigma}_z})|\alpha\rangle . \end{aligned} \tag{4.14}$$

Now $\tilde{D}(\beta)$ transforms the states $|\alpha,0\rangle$ and $|\alpha,1\rangle$ as follows:

$$\tilde{D}(\beta)|\alpha,0\rangle = D(-i\beta e^{i\frac{\pi}{2}})|\alpha,0\rangle = D(\beta)|\alpha,0\rangle , \tag{4.15a}$$

$$\tilde{D}(\beta)|\alpha,1\rangle = D(-i\beta e^{-i\frac{\pi}{2}})|\alpha,1\rangle = D(-\beta)|\alpha,1\rangle . \tag{4.15b}$$

4.2. 1D QUANTUM RANDOM WALK WITH CONTROLLED DISPLACEMENTS

We can now perform a one-dimensional QRW over the coherent states $|n\alpha\rangle$ for $n \in \mathbb{N}$ and $\alpha \in \mathbb{R}$ by first applying a controlled displacement $\tilde{D}(\alpha)$ followed by a Hadamard flip on the qubit for each step of the walk. This is a walk on the horizontal axis of phase space. Note that we should choose α large enough such that the states are well distinguishable and do not overlap too much, as we saw in Equation (4.9). The sequence of gates needed to perform this is shown in Figure 4.2.

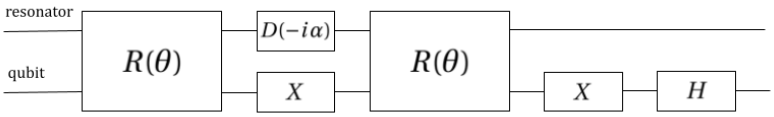

Figure 4.2: Sequence of gates applied to a resonator and a qubits to perform a step of the 1D QRW on coherent states in phase space from the state $|n\alpha\rangle$ to the states $|(n\pm 1)\alpha\rangle$, with $\alpha \in \mathbb{R}$ and $n \in \mathbb{N}$. $R(\theta)$ represents a conditional rotation $e^{-i\theta\hat{a}^\dagger\hat{a}\hat{\sigma}_z}$ with $\theta = \frac{\pi}{2}$.

We can also walk over the coherent states $|im\alpha\rangle$ for $m \in \mathbb{N}$ and $\alpha \in \mathbb{R}$ if we replace the unconditional displacement $D(-i\beta)$ in the controlled displacement sequence by $\tilde{D}$ by $D(-\beta)$. In this case the walk moves on the vertical axis of phase space.

The 1D QRW with controlled displacements behaves the same as the 1D discrete QRW we saw in Chapter 2. The unitary operator U for each step of the walk is given by:

$$U = D(\alpha) \otimes |+\rangle\langle 0| + D(\alpha) \otimes |-\rangle\langle 1|. \tag{4.16}$$

The coefficients needed to calculate the probability distribution of the 1D QRW with controlled displacements after t steps may be derived by Equation (2.25), with initial conditions Equation (2.26). The probability $P_t(\alpha_0 + n\alpha)$ of measuring a walk that starts in initial state $|\Psi_0\rangle = |\alpha_0\rangle \otimes (a|0\rangle + b|1\rangle)$ in a coherent state $|\alpha_0 + n\alpha\rangle$ after t steps is given by Equation (2.28).

4.3. 2D QUANTUM RANDOM WALKS WITH CONTROLLED DISPLACEMENTS

Since the walk is performed in the two-dimensional phase space we can also perform a two-dimensional walk on a grid. The walk then moves over the coherent states $|n\alpha + im\beta\rangle$ for $n, m \in \mathbb{N}$. This is done by first performing the horizontal controlled displacement $D_{\text{hor}}(\alpha) = R^\dagger(\theta)_1 D(-i\alpha) R(\theta)_1$ as shown in Figure 4.2, and then a vertical controlled displacement $D_{\text{vert}}(i\beta) = R^\dagger(\theta)_2 D(-\beta) R(\theta)_2$ for $\theta = \frac{\pi}{2}$. We need two qubits to be able to do

this, where qubit 1 corresponds to the horizontal step of the walk and qubit 2 to the vertical step of the walk. The rotation $R(\theta)_1$ is achieved by dispersively coupling the resonator to qubit 1 and the rotation $R(\theta)_2$ by dispersive coupling the resonator to qubit 2. Note that we should choose α and β large enough such that the coherent states of the walk are well distinguishable and do not overlap too much, as we saw in Equation (4.9). The sequence of gates that are applied to the resonator and qubits are shown in Figure 4.3.

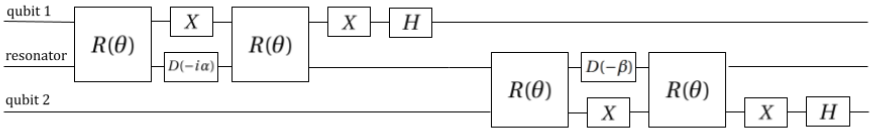

Figure 4.3: Sequence of gates applied to a resonator and 2 qubits to perform a step of the 2D QRW on coherent states in phase space from the state $|n\alpha + im\beta\rangle$ to the states $|(n\pm1)\alpha + i(m\pm1)\beta\rangle$ with $\alpha, \beta \in \mathbb{R}$ and $n, m \in \mathbb{N}$. $R(\theta)$ represents a conditional rotation $e^{-i\theta\hat{a}^\dagger\hat{a}\hat{\sigma}_z}$.

This corresponds to a walk that moves from coherent state $|n\alpha + im\beta\rangle$ to the states $|(n\pm1)\alpha + i(m\pm1)\beta\rangle$, which is a movement similar to the walk on the 2D grid we shortly viewed in Chapter 2. Now that the QRW moves in phase space using displacements instead of position space, we have to account for extra phase factors between different parts of the walk that arise because of the phase differences for sequences of displacements as we saw in Equation (4.3). This is because the operators $D(\alpha)$ and $D(\beta)$ do not commute. In the one-dimensional case of the walk in phase space these phase differences do not arise because on the horizontal axis of phase space we have that the extra phase term in Equation (4.3) is equal to 1 because α and $n\alpha$ are both real such that $D(\pm\alpha)D(n\alpha) = D((n\pm1)\alpha)$. In the two-dimensional case we can choose the size of the grid such that $D(\alpha)$ and $D(\beta)$ commute. We first derive a general formula to calculate the coefficients of the 2D QRW using a recursion. Then we study the properties of the walk for values $\alpha\cdot\beta$ such that the extra phase differences do not influence the walk using numerical simulations. Finally we study how extra phase factors affect the properties of the walk for different values of $\alpha\cdot\beta$ in these numerical simulations.

4.3.1. DERIVATION OF THE COEFFICIENTS OF THE RECURSIVE WALK IN 2D

The unitary operator U for a step of the 2D walk is given by

$$\begin{aligned} U =& D(i\beta)D(\alpha)\otimes|{+}{+}\rangle\langle 00| + D(-i\beta)D(\alpha)\otimes|{+}{-}\rangle\langle 01| \\ &+ D(i\beta)D(-\alpha)\otimes|{-}{+}\rangle\langle 10| + D(-i\beta)D(-\alpha)\otimes|{-}{-}\rangle\langle 11|. \end{aligned} \tag{4.17}$$

From this we can see that the operator U^t will be of the form

$$\begin{aligned} U^t = \left(\frac{1}{2}\right)^{t-1} \Big(& D^t_{++00} \otimes |++\rangle\langle 00| + D^t_{+-00} \otimes |+-\rangle\langle 00| + D^t_{-+00} \otimes |-+\rangle\langle 00| + D^t_{--00} \otimes |--\rangle\langle 00| \\ & + (D^t_{++01} \otimes |++\rangle\langle 01| + D^t_{+-01} \otimes |+-\rangle\langle 01| + D^t_{-+01} \otimes |-+\rangle\langle 01| + D^t_{--01} \otimes |--\rangle\langle 01| \\ & + (D^t_{++10} \otimes |++\rangle\langle 10| + D^t_{+-10} \otimes |+-\rangle\langle 10| + D^t_{-+10} \otimes |-+\rangle\langle 10| + D^t_{--10} \otimes |--\rangle\langle 10| \\ & + (D^t_{++11} \otimes |++\rangle\langle 11| + D^t_{+-11} \otimes |+-\rangle\langle 11| + D^t_{-+11} \otimes |-+\rangle\langle 11| + D^t_{--11} \otimes |--\rangle\langle 11| \Big) \end{aligned} \tag{4.18}$$

with $D_{\pm\pm jk} = \sum_{n,m} c^t_{nm,\pm\pm jk} D(n\alpha + im\beta)$, where $j,k \in 0,1$ and $n,m \in \mathbb{Z}$.

From Equation (4.3) it follows that

$$\begin{aligned} D(i\beta)D(\alpha)D(n\alpha+im\beta) &= e^{-im\alpha\beta}e^{i(n+1)\alpha\beta}D((n+1)\alpha+i(m+1)\beta) \\ D(-i\beta)D(\alpha)D(n\alpha+im\beta) &= e^{-im\alpha\beta}e^{-i(n+1)\alpha\beta}D((n+1)\alpha+i(m-1)\beta) \\ D(i\beta)D(-\alpha)D(n\alpha+im\beta) &= e^{im\alpha\beta}e^{i(n-1)\alpha\beta}D((n-1)\alpha+i(m+1)\beta) \\ D(-i\beta)D(-\alpha)D(n\alpha+im\beta) &= e^{im\alpha\beta}e^{-i(n-1)\alpha\beta}D((n-1)\alpha+i(m-1)\beta) \end{aligned} \tag{4.19}$$

which we can use to calculate how the coefficients $c^{t+1}_{nm,\pm\pm jk}$ can be calculated from the $c^t_{nm,\pm jk}$'s. We use the following notation to shorten the equations as follows:

$$\begin{aligned} e^{i(n-m+1)\alpha\beta} &= e^{\phi_1} \\ e^{i(-n-m-1)\alpha\beta} &= e^{\phi_2} \\ e^{i(n+m-1)\alpha\beta} &= e^{\phi_3} \\ e^{i(-n+m+1)\alpha\beta} &= e^{\phi_4} \end{aligned} \tag{4.20}$$

$$
\begin{aligned}
c^{t+1}_{nm,++00} &= \left(c^{t}_{(n-1)(m-1),++00} + c^{t}_{(n-1)(m-1),+-00} + c^{t}_{(n-1)(m-1),-+00} + c^{t}_{(n-1)(m-1),--00}\right)\cdot e^{\phi_1}\\
c^{t+1}_{nm,++01} &= \left(c^{t}_{(n-1)(m-1),++01} + c^{t}_{(n-1)(m-1),+-01} + c^{t}_{(n-1)(m-1),-+01} + c^{t}_{(n-1)(m-1),--01}\right)\cdot e^{\phi_1}\\
c^{t+1}_{nm,++10} &= \left(c^{t}_{(n-1)(m-1),++10} + c^{t}_{(n-1)(m-1),+-10} + c^{t}_{(n-1)(m-1),-+10} + c^{t}_{(n-1)(m-1),--10}\right)\cdot e^{\phi_1}\\
c^{t+1}_{nm,++11} &= \left(c^{t}_{(n-1)(m-1),++11} + c^{t}_{(n-1)(m-1),+-11} + c^{t}_{(n-1)(m-1),-+11} + c^{t}_{(n-1)(m-1),--11}\right)\cdot e^{\phi_1}\\
\\
c^{t+1}_{nm,+-00} &= \left(c^{t}_{(n-1)(m+1),++00} - c^{t}_{(n-1)(m+1),+-00} + c^{t}_{(n-1)(m+1),-+00} - c^{t}_{(n-1)(m+1),--00}\right)\cdot e^{\phi_2}\\
c^{t+1}_{nm,+-01} &= \left(c^{t}_{(n-1)(m+1),++01} - c^{t}_{(n-1)(m+1),+-01} + c^{t}_{(n-1)(m+1),-+01} - c^{t}_{(n-1)(m+1),--01}\right)\cdot e^{\phi_2}\\
c^{t+1}_{nm,+-10} &= \left(c^{t}_{(n-1)(m+1),++10} - c^{t}_{(n-1)(m+1),+-10} + c^{t}_{(n-1)(m+1),-+10} - c^{t}_{(n-1)(m+1),--10}\right)\cdot e^{\phi_2}\\
c^{t+1}_{nm,+-11} &= \left(c^{t}_{(n-1)(m+1),++11} - c^{t}_{(n-1)(m+1),+-11} + c^{t}_{(n-1)(m+1),-+11} - c^{t}_{(n-1)(m+1),--11}\right)\cdot e^{\phi_2}\\
\\
c^{t+1}_{nm,-+00} &= \left(c^{t}_{(n+1)(m-1),++00} + c^{t}_{(n+1)(m-1),+-00} - c^{t}_{(n+1)(m-1),-+00} - c^{t}_{(n+1)(m-1),--00}\right)\cdot e^{\phi_3}\\
c^{t+1}_{nm,-+01} &= \left(c^{t}_{(n+1)(m-1),++01} + c^{t}_{(n+1)(m-1),+-01} - c^{t}_{(n+1)(m-1),-+01} - c^{t}_{(n+1)(m-1),--01}\right)\cdot e^{\phi_3}\\
c^{t+1}_{nm,-+10} &= \left(c^{t}_{(n+1)(m-1),++10} + c^{t}_{(n+1)(m-1),+-10} - c^{t}_{(n+1)(m-1),-+10} - c^{t}_{(n+1)(m-1),--10}\right)\cdot e^{\phi_3}\\
c^{t+1}_{nm,-+11} &= \left(c^{t}_{(n+1)(m-1),++11} + c^{t}_{(n+1)(m-1),+-11} - c^{t}_{(n+1)(m-1),-+11} - c^{t}_{(n+1)(m-1),--11}\right)\cdot e^{\phi_3}\\
\\
c^{t+1}_{nm,--00} &= \left(c^{t}_{(n+1)(m+1),++00} - c^{t}_{(n+1)(m+1),+-00} - c^{t}_{(n+1)(m+1),-+00} + c^{t}_{(n+1)(m+1),--00}\right)\cdot e^{\phi_4}\\
c^{t+1}_{nm,--01} &= \left(c^{t}_{(n+1)(m+1),++01} - c^{t}_{(n+1)(m+1),+-01} - c^{t}_{(n+1)(m+1),-+01} + c^{t}_{(n+1)(m+1),--01}\right)\cdot e^{\phi_4}\\
c^{t+1}_{nm,--10} &= \left(c^{t}_{(n+1)(m+1),++10} - c^{t}_{(n+1)(m+1),+-10} - c^{t}_{(n+1)(m+1),-+10} + c^{t}_{(n+1)(m+1),--10}\right)\cdot e^{\phi_4}\\
c^{t+1}_{nm,--11} &= \left(c^{t}_{(n+1)(m+1),++11} - c^{t}_{(n+1)(m+1),+-11} - c^{t}_{(n+1)(m+1),-+11} + c^{t}_{(n+1)(m+1),--11}\right)\cdot e^{\phi_4}
\end{aligned}
\tag{4.21}
$$

where we have that

$$
\begin{aligned}
c^{1}_{nm,++00} &= \begin{cases} e^{i\alpha\beta} & \text{for } n=1, m=1,\\ 0 & \text{otherwise.}\end{cases}\\
c^{1}_{nm,+-01} &= \begin{cases} e^{-i\alpha\beta} & \text{for } n=1, m=-1,\\ 0 & \text{otherwise.}\end{cases}\\
c^{1}_{nm,-+10} &= \begin{cases} e^{-i\alpha\beta} & \text{for } n=-1, m=1,\\ 0 & \text{otherwise.}\end{cases}\\
c^{1}_{nm,--11} &= \begin{cases} e^{i\alpha\beta} & \text{for } n=-1, m=-1,\\ 0 & \text{otherwise.}\end{cases}
\end{aligned}
\tag{4.22}
$$

and the other $c^{1}_{nm,\pm\pm jk} = 0$.

From these coefficients the probability distribution of the walk a walk in initial position

$|\Psi_0\rangle = |0\rangle \otimes (a|0\rangle_1 + b|1\rangle_1)(c|0\rangle_2 + d|1\rangle_2)$ after t steps may be obtained by using the following equation:

$$
\begin{aligned}
&P_t(n\alpha + im\beta) = \\
&\frac{1}{4^t}\Big(\Big|\begin{matrix} ac\big(c^t_{nm,++00} + c^t_{nm,+-00} + c^t_{nm,-+00} + c^t_{nm,--00}\big) + ad\big(c^t_{nm,++01} + c^t_{nm,+-01} + c^t_{nm,-+01} + c^t_{nm,--01}\big) \\ +bc\big(c^t_{nm,++10} + c^t_{nm,+-10} + c^t_{nm,-+10} + c^t_{nm,--10}\big) + bd\big(c^t_{nm,++11} + c^t_{nm,+-11} + c^t_{nm,-+11} + c^t_{nm,--11}\big)\end{matrix}\Big|^2 \\
&+\Big|\begin{matrix} ac\big(c^t_{nm,++00} - c^t_{nm,+-00} + c^t_{nm,-+00} - c^t_{nm,--00}\big) + ad\big(c^t_{nm,++01} - c^t_{nm,+-01} + c^t_{nm,-+01} - c^t_{nm,--01}\big) \\ +bc\big(c^t_{nm,++10} - c^t_{nm,+-10} + c^t_{nm,-+10} - c^t_{nm,--10}\big) + bd\big(c^t_{nm,++11} - c^t_{nm,+-11} + c^t_{nm,-+11} - c^t_{nm,--11}\big)\end{matrix}\Big|^2 \\
&+\Big|\begin{matrix} ac\big(c^t_{nm,++00} + c^t_{nm,+-00} - c^t_{nm,-+00} - c^t_{nm,--00}\big) + ad\big(c^t_{nm,++01} + c^t_{nm,+-01} - c^t_{nm,-+01} - c^t_{nm,--01}\big) \\ +bc\big(c^t_{nm,++10} + c^t_{nm,+-10} - c^t_{nm,-+10} - c^t_{nm,--10}\big) + bd\big(c^t_{nm,++11} + c^t_{nm,+-11} - c^t_{nm,-+11} - c^t_{nm,--11}\big)\end{matrix}\Big|^2 \\
&+\Big|\begin{matrix} ac\big(c^t_{nm,++00} - c^t_{nm,+-00} - c^t_{nm,-+00} + c^t_{nm,--00}\big) + ad\big(c^t_{nm,++01} - c^t_{nm,+-01} - c^t_{nm,-+01} + c^t_{nm,--01}\big) \\ +bc\big(c^t_{nm,++10} - c^t_{nm,+-10} - c^t_{nm,-+10} + c^t_{nm,--10}\big) + bd\big(c^t_{nm,++11} - c^t_{nm,+-11} - c^t_{nm,-+11} + c^t_{nm,--11}\big)\end{matrix}\Big|^2\Big)
\end{aligned}
\tag{4.23}
$$

4.3.2. RESULTS OF COMMUTING QUANTUM RANDOM WALKS ON THE 2D GRID IN PHASE SPACE

First we look at the case where the phases between steps of the walk cancel. The probability distribution of the QRW on the 2D grid in phase space should then look like a regular 2D QRW. From Equation (4.3) it follows that

$$D(\alpha)D(i\beta) = e^{\frac{-i\alpha\beta - i\alpha\beta}{2}} D(\alpha + i\beta) = e^{-2i\alpha\beta} D(i\beta)D(\alpha), \tag{4.24}$$

$$D(\alpha)D(-i\beta) = e^{\frac{i\alpha\beta + i\alpha\beta}{2}} D(\alpha - i\beta) = e^{2i\alpha\beta} D(-i\beta)D(\alpha), \tag{4.25}$$

where $\alpha, \beta \in \mathbb{R}$. A similar calculation can be done for $D(-\alpha)D(i\beta)$ and $D(-\alpha)D(-i\beta)$ such that we find that for $\alpha \cdot \beta = 0 \bmod \pi$ we have that $D(\pm\alpha)$ and $D(\pm i\beta)$ commute. Therefore a sequence of displacements $D(\pm i\beta)D(\pm\alpha)...D(\pm i\beta)D(\alpha)$ in the QRW may be simply rewritten to $D(\pm i\beta)...D(\pm i\beta)D(\pm\alpha)...D(\pm\alpha)$. In this case we can calculate the probability of measuring the 2D QRW in the coherent state $|n\alpha + im\beta\rangle$ after t steps by multiplying the probability of measuring the 1D QRW after t steps in the coherent state $|n\alpha\rangle$ and $|m\alpha\rangle$:

$$P_t(n\alpha + im\beta)_{2D} = P_t(n\alpha)_{1D} P_t(m\alpha)_{1D} \tag{4.26}$$

Thus when $D(\pm\alpha)$ and $D(\pm i\beta)$ commute, the 2D QRW consists of two uncoupled 1D QRW's. For $\alpha \cdot \beta = 0 \mod \pi$ we then achieve the quantum version of the simple 2D CRW we saw in Chapter 2.

Note that for all values of $\alpha \cdot \beta$ we may add a multiple of 2π such that we can adjust the size of the displacements α and β such that the coherent states $|n\alpha + im\beta\rangle$ do not overlap for different n, m.

The distribution of the commuting QRW on the 2D grid of coherent states after t steps,

with symmetric initial state

$$|\Psi_0\rangle = |0\rangle \otimes \tfrac{1}{2}(|0\rangle_1 + i\,|1\rangle_1)(|0\rangle_2 + i\,|1\rangle_2) \tag{4.27}$$

is plotted for $t = 25, 50, 75, 100$ in Figure 4.4. The whole evolution of 100 steps of the commuting 2D walk is given in this linked animated movie. Each frame of the animation corresponds to one step of the 2D QRW as in Figure 4.3. The color scale changes throughout the animation for presentation purposes.

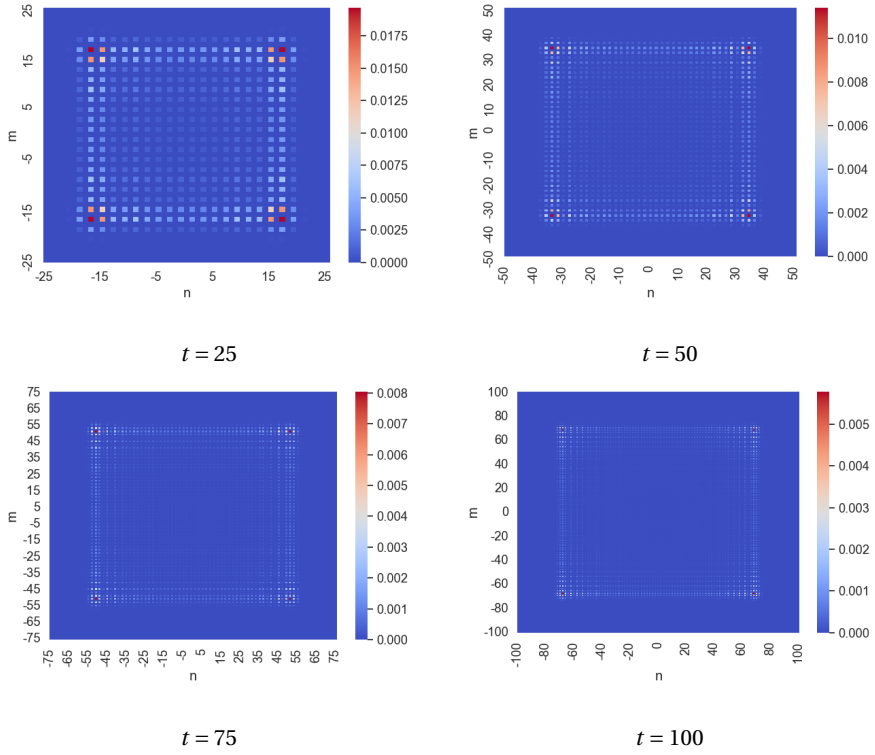

Figure 4.4: Probability distribution of the commuting QRW on the 2D grid of coherent states after t steps, with initial position $|\Psi_0\rangle$

The expected value of the x and y position of the commuting walk is equal to 0, just like in the case of a 1D QRW. The variance of the x and y position of the commuting walk are equal to the variance of the 1D QRW we saw in Figure 2.7.

An interesting observation from the numerical simulations of the 2D QRW is that we obtain the same probability distributions and animated evolution of the walk for $\alpha \cdot \beta = \frac{\pi}{2}$. It seems from the simulations that the walk also commutes for values $\alpha \cdot \beta = 0 \bmod \frac{\pi}{2}$. The distribution of the commuting QRW on the 2D grid of coherent states after t steps, with the symmetric initial state from Equation (4.27) for $\alpha \cdot \beta = \frac{\pi}{2}$, is plotted for $t = 50, 100$ in Figure 4.5. These figures look the same as Figure 4.4 for $t = 50, 100$.

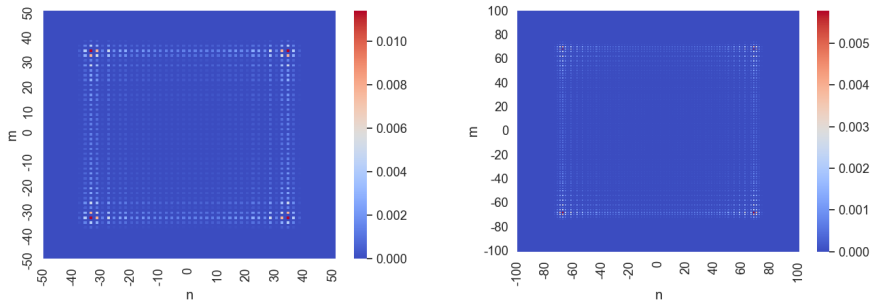

$t = 50$ $t = 100$

Figure 4.5: Probability distribution of the QRW with $\alpha \cdot \beta = \frac{\pi}{2}$ on the 2D grid of coherent states after t steps, with initial position $|\Psi_0\rangle$.

The whole evolution of 100 steps of the probability distribution for $\alpha \cdot \beta = \frac{\pi}{2}$ is given in this linked animated movie, which looks the same as the evolution of 100 steps of the commuting QRW. Subtracting the probabilities of the distribution for $\alpha \cdot \beta = \frac{\pi}{2}$ after t steps from the distribution for $\alpha \cdot \beta = 0 \bmod \pi$ after t steps, gives a value of the order of a floating point error.

4.3.3. RESULTS OF NONCOMMUTING QUANTUM RANDOM WALKS ON THE 2D GRID IN PHASE SPACE

For choices of $\alpha \cdot \beta \neq 0 \bmod \frac{\pi}{2}$ we expect the phase factors $e^{\phi_1}, e^{\phi_2}, e^{\phi_3}, e^{\phi_4}$ in Equation (4.21) to influence the behaviour of the QRW.

If we choose $\alpha \cdot \beta$ equal to a fraction of π such as $\alpha \cdot \beta = \frac{\pi}{3}$ or $\frac{\pi}{4}$, we see some interesting patterns arise. The probability distribution of these walks for $t = 50, 100$ are plotted in the figure below. A linked animated movie of the evolution of the walks is given for $\alpha \cdot \beta = \pi/3$ and $\alpha \cdot \beta = \pi/4$. Clearly a different pattern than the pattern of the commuting walk arises. Additionally, it seems that the walk did not propagate as far as the QRW for $\alpha \cdot \beta = 0 \bmod \frac{\pi}{2}$. This is indeed visible in a plot of the variance of the x-coordinate of the QRW's in Figure 4.7 for several different values of $\alpha \cdot \beta$ that are a fraction of π, together with the CRW.

A plot of the variance of the y-coordinate of the walk gives the same image, which makes sense as the plots in Figure 4.6 seem symmetric in the x and y direction. In this chapter we will only study the variance of the x-coordinate of the walk.

From Figure 4.7 it seems that the walk for $\alpha \cdot \beta = \frac{\pi}{3}, \frac{\pi}{6}, \frac{2\pi}{3}$ and $\frac{5\pi}{6}$ have equal variances and are plotted on top of each other. Animations of the evolution of the walks for these values of $\alpha \cdot \beta$ appear to be equal as well. For $\alpha \cdot \beta = \frac{\pi}{4}, \frac{3\pi}{4}$ the variances also appear equal plotted on top of each other and generate the same animation of the evolution. It seems

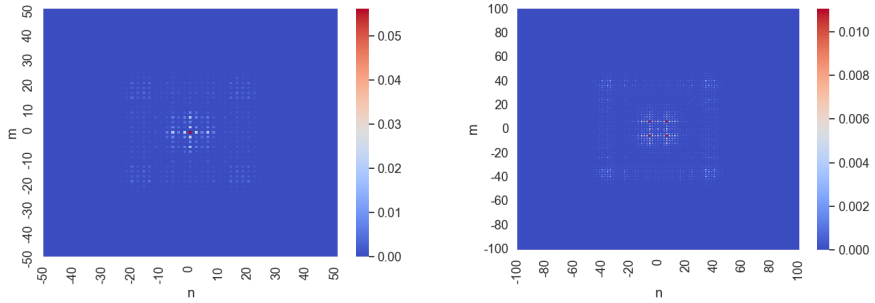

$t = 50$ $t = 100$

Figure 4.6: Probability distribution of the noncommuting QRW with $\alpha \cdot \beta = \frac{\pi}{3}$ on the 2D grid of coherent states after t steps, with initial position $|\Psi_0\rangle$.

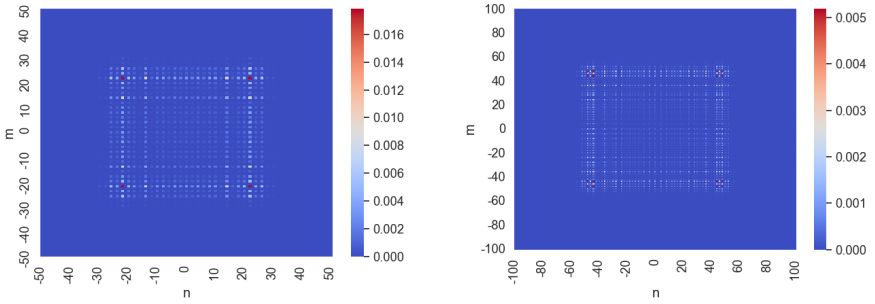

$t = 50$ $t = 100$ steps

Probability distribution of the noncommuting QRW with $\alpha \cdot \beta = \frac{\pi}{4}$ on the 2D grid of coherent states after t steps, with initial position $|\Psi_0\rangle$.

that the value of $\alpha \cdot \beta$ is not the variable responsible for the behaviour of the QRW, but $|\alpha \cdot \beta - 0 \bmod \frac{\pi}{2}|$ is what matters more.

A log-log plot of σ_x^2 for $\alpha \cdot \beta = 0, \frac{\pi}{6}$ and $\frac{\pi}{4}$ and the CRW are shown in Figure 4.8. It seems from these figures that the log-log slope of the variances is equal for $\alpha \cdot \beta = 0, \frac{\pi}{6}$ and $\frac{\pi}{4}$ and thus $\sigma_x^2 \sim t^2$ for all of these values of $\alpha \cdot \beta$. The vertical shift between the three plots shows that the factor a in the function $\sigma_x^2 = at^2$ is different for the different values of $\alpha \cdot \beta$. It is remarkable that the graphs for $\alpha \cdot \beta = \frac{\pi}{6}$ and $\frac{\pi}{4}$ show noisy behaviour around t=10.

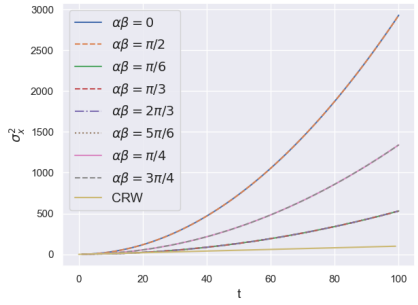

Figure 4.7: Variance of the x-coordinate of the QRW for several values of $\alpha \cdot \beta$ on the 2D grid of coherent states, plotted against number of steps, with initial position $|\Psi_0\rangle$.

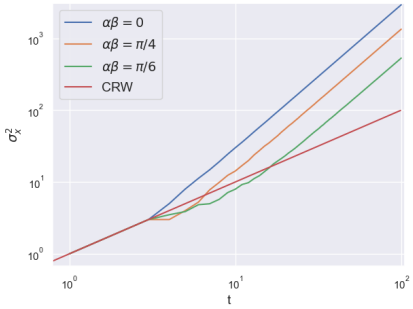

Figure 4.8: Variance of the x-coordinate of the QRW for several values of $\alpha \cdot \beta$ on the 2D grid of coherent states, plotted against number of steps on a log-log scale, with initial position $|\Psi_0\rangle$.

To explore the hypothesis that $|\alpha \cdot \beta - 0 \bmod \frac{\pi}{2}|$ (i.e. the distance of $\alpha \cdot \beta$ from integer multiples of $\frac{\pi}{2}$) is the variable responsible for different behaviours of the walk, a plot is shown for equally spaced and small fractions of π. In Figure 4.9 σ_x^2 is plotted for 2D QRW's with $\alpha \cdot \beta = 0, \frac{\pi}{24}, \frac{\pi}{12}, \frac{\pi}{8}, \frac{\pi}{6}, \frac{5\pi}{24}, \frac{\pi}{4}$, and in Figure 4.10 for $\alpha \cdot \beta = \frac{\pi}{4}, \frac{7\pi}{24}, \frac{\pi}{3}, \frac{3\pi}{8}, \frac{5\pi}{12}, \frac{11\pi}{24}, \frac{\pi}{2}$, but in reverse order such that the colors of the graphs correspond to the same distance $|\alpha \cdot \beta - 0 \bmod \frac{\pi}{2}|$. Indeed these graphs look exactly the same.

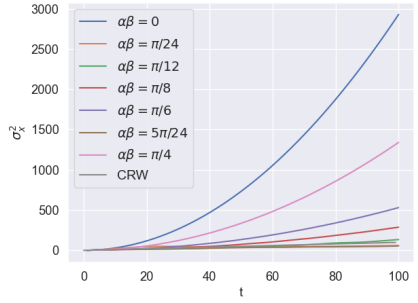

Figure 4.9: Variance of the noncommuting QRW for several equally spaced values of $\alpha \cdot \beta$ between 0 and $\frac{\pi}{4}$ on the 2D grid of coherent states, plotted against number of steps, with initial position $|\Psi_0\rangle$.

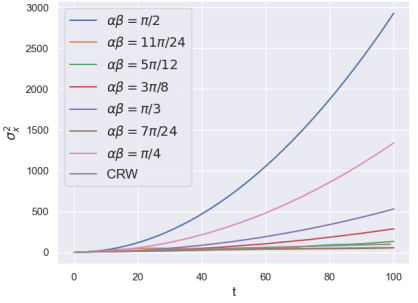

Figure 4.10: Variance of the noncommuting QRW for several equally spaced values of $\alpha \cdot \beta$ between $\frac{\pi}{4}$ and $\frac{\pi}{2}$ on the 2D grid of coherent states, plotted against number of steps, with initial position $|\Psi_0\rangle$.

A zoomed in plot of the variances of the QRW for the values $\alpha \cdot \beta = \frac{\pi}{24}, \frac{\pi}{12}, \frac{\pi}{8}, \frac{5\pi}{24}$ and the variance of the 1D CRW is shown in Figure 4.11. The graph for $\alpha \cdot \beta = \frac{\pi}{8}$ seems to show a proportionality $\sigma_x^2 \sim t^2$. However, investigation of the behaviour of this walk after $t = 100$ should be performed to be more conclusive. The graphs for other values of $\alpha \cdot \beta$ show behaviour that does not seem to have a clear proportionality with the number of steps

t and that is not monotone. The variance of these walks is close to the variance of the CRW and sometimes even smaller. This seems to indicate that for values of $\alpha \cdot \beta$ that are not equal to $\pm\frac{\pi}{6}$ mod $\frac{\pi}{2}$ or $\pm\frac{\pi}{4}$ mod $\frac{\pi}{2}$, the variance of the QRW does not show the same quantum behaviour.

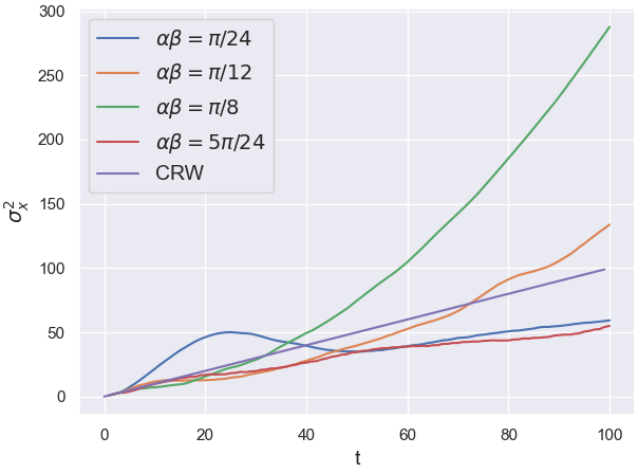

Figure 4.11: Zoomed in plot of variance of the noncommuting QRW for several values of $\alpha \cdot \beta$ from Figure 4.9 on the 2D grid of coherent states, plotted against number of steps, with initial position $|\Psi_0\rangle$.

To investigate this idea further we study some values of $\alpha \cdot \beta$ that are not of the form $q\pi$ for $q \in \mathbb{Q}$. For $\alpha \cdot \beta = 0.001 \bmod \frac{\pi}{2}$ the probability distribution after 100 steps looks very similar to the commuting 2D QRW as can be seen in Figure 4.12. This could be explained by the fact that the phase factor is so small that interference is not clearly visible. For $\alpha \cdot \beta = 0.01 \bmod \frac{\pi}{2}$ the probability distribution after 100 steps still looks very similar to the commuting 2D QRW, however a slight curvature around the otherwise rectangular shape of the peaks of the distribution is visible as can be seen in Figure 4.13. For $\alpha \cdot \beta = 0.1 \bmod \frac{\pi}{2}$ the probability distribution after 100 steps has become centered at the origin of the grid.

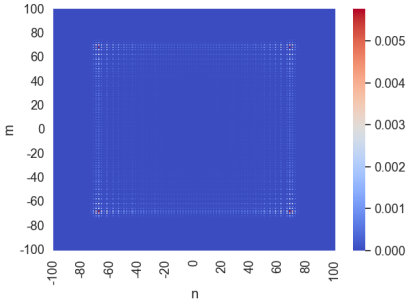

Figure 4.12: Probability distribution of the noncommuting QRW with $\alpha \cdot \beta = 0.001$ on the 2D grid of coherent states after $t = 100$ steps, with initial position $|\Psi_0\rangle$.

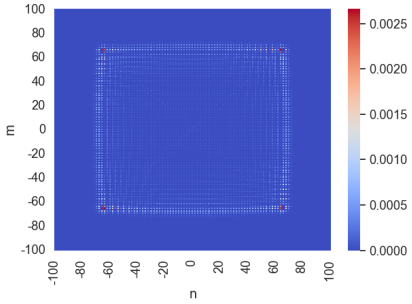

Figure 4.13: Probability distribution of the noncommuting QRW with $\alpha \cdot \beta = 0.001$ on the 2D grid of coherent states after $t = 100$ steps, with initial position $|\Psi_0\rangle$.

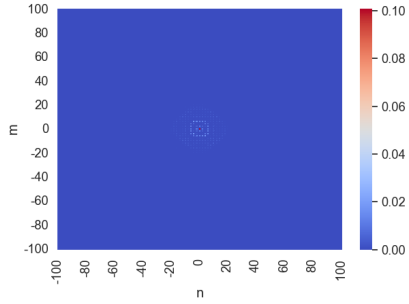

Figure 4.14: Probability distribution of the noncommuting QRW with $\alpha \cdot \beta = 0.1$ on the 2D grid of coherent states after $t = 100$ steps, with initial position $|\Psi_0\rangle$.

If we look at the evolution of the walk for $\alpha \cdot \beta = 0.05$ in Figure 4.15 we see that it starts rectangular, then circular, then collapses to a distribution centered closely around the origin. For extra visibility these plots are focussed only on the probability amplitudes for $n = [-50, 50]$ $m = [-50, 50]$. Outside of this area the probability amplitudes are (approximately) equal to zero for all 100 steps of the walk. Note that the scale of the heatmaps differs for each figure for presentation purposes. The whole evolution of 100 steps of the probability distribution for $\alpha \cdot \beta = 0.05$ is given in this linked animated movie.

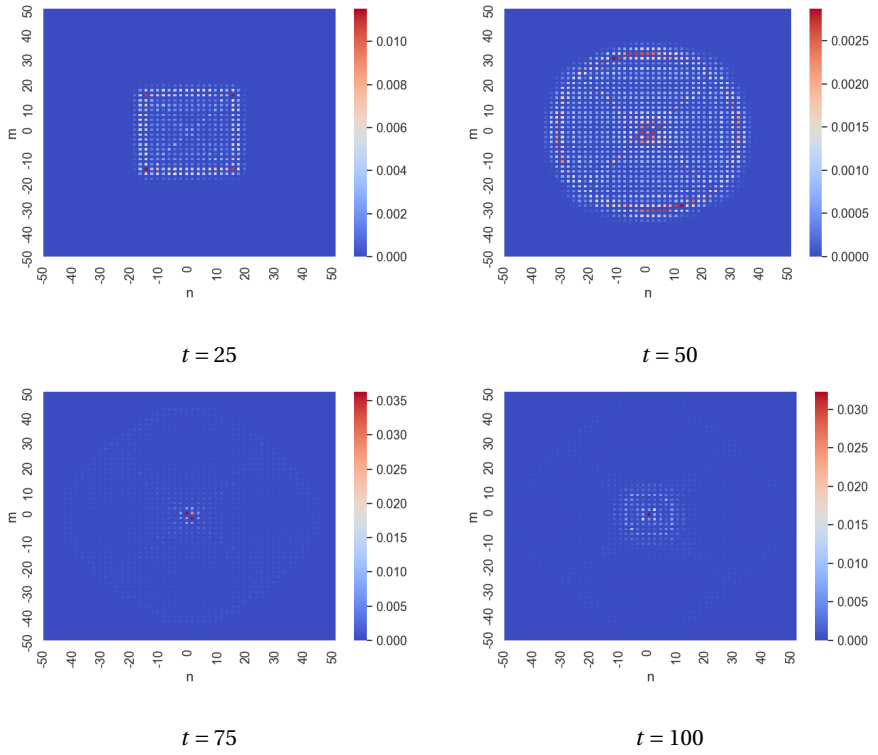

Figure 4.15: Probability distribution of the noncommuting QRW with $\alpha \cdot \beta = 0.05$ on the 2D grid of coherent states after t steps, with initial position $|\Psi_0\rangle$.

We also see this when plotting the variance of the walk for different values of $\alpha \cdot \beta$ that are not rational multiplications of π. For values $\alpha \cdot \beta = 0.001, 0.005, 0.01$ we see in Figure 4.16 that the variance is close to the commuting 2D QRW. The phase differences are small and do not accumulate to a collapse before $t = 100$ steps. The variances of these walks are very close to the commuting QRW, which indicates that for experimental implementations of the walk in this setup for $t < 100$ steps, a small deviation in the displacements α and β is allowed and the quantum behaviour of the walk will still be visible. Hoewever, it might be the case that the walk eventually collapses for larger t.

A zoomed in plot of σ_x^2 for values $\alpha \cdot \beta = 0.05, 0.1, 0.5$ is shown in Figure 4.17. For these walks it seems that σ_x^2 is not monotone and there is no clear relationship with the number of steps t. It seems that the walks collapse after some number of steps. The behaviour of these walks is closer to a CRW and in some cases σ_x^2 is even smaller than the CRW. The phases accumulate more quickly when $\alpha \cdot \beta$ is far from 0 mod $\frac{\pi}{2}$. The variance is also smaller compared to the variance of the walk for values of $\alpha \cdot \beta$ such as $\pm\frac{\pi}{6}$ mod $\frac{\pi}{2}$ or $\pm\frac{\pi}{4}$ mod $\frac{\pi}{2}$, even though the distance $|\alpha \cdot \beta - 0 \bmod \frac{\pi}{2}|$ is similar. An explanation for this could be that the phases in the walk for $\alpha \cdot \beta = \pm\frac{\pi}{6}$ mod $\frac{\pi}{2}$ or $\pm\frac{\pi}{4}$ mod $\frac{\pi}{2}$ accumulate to rational and integer multiples of π, such that quantum interference is still visible. This might explain why we see that the walk collapses quickly to a walk centered at the origin for $\alpha \cdot \beta = 0.1, 0.5$.

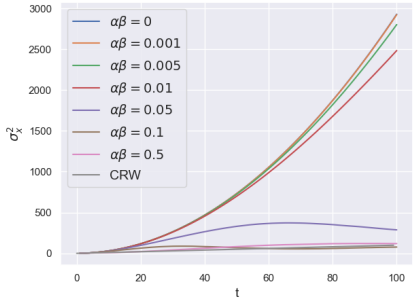

Figure 4.16: Variance of the noncommuting QRW for several values of $\alpha \cdot \beta$ close to 0 mod $\frac{\pi}{2}$ on the 2D grid of coherent states, plotted against number of steps, with initial position $|\Psi_0\rangle$.

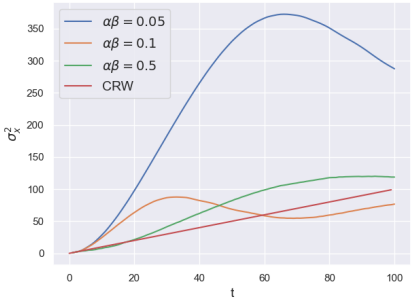

Figure 4.17: Variance of the noncommuting QRW for several values of $\alpha \cdot \beta$ a bit further from 0 mod $\frac{\pi}{2}$ on the 2D grid of coherent states, plotted against number of steps, with initial position $|\Psi_0\rangle$.

5

DISCUSSION

5.1. DISCUSSION OF PHYSICAL LIMITATIONS OF THE IMPLEMENTATION OF A QRW IN PHASE SPACE

A QRW is always subject to decoherence, caused by interaction of the surrounding environment. This can cause the walk to behave more like a CRW. A few effects that occur are *dephasing*, *relaxation* and *photon loss*, which will shortly be discussed. Furthermore, we will look at coherence times of the gate sequence setup we suggested to perform the QRW on the 2D grid in phase space with superconducting qubits in circuit-QED.

DEPHASING

Suppose that the QRW is in the state $|\Psi_t\rangle$ at some time t. We may also write the state in terms of its density matrix $\rho = |\Psi_t\rangle\langle\Psi_t|$. Dephasing is a form of decoherence which can mathematically be described by the off diagonal elements of the density matrix ρ changing to zero. This means that a state $|+\rangle = (|0\rangle + |1\rangle)/\sqrt{2}$ is no longer a superposition of the state $|0\rangle$ and $|1\rangle$, but turned into a state $|0\rangle$ or $|1\rangle$ with a probability of 0.5 for either of the two states. In the QRW, dephasing of the qubit corresponds to a classical step of the walk in which a classical coin decides if a step to the left or right occurs. The rate at which dephasing occurs is called T_2. If dephasing occurs in between or during steps, the quantum effect of the walk will be disturbed and a more classical distribution of the walk appears. The effect of dephasing in QRW's has been researched by introducing non unitary evolution in a numerical model of the QRW. [19][20]

RELAXATION

Another form of quantum decoherence is relaxation of a qubit. Relaxation means that the higher energy state of the qubit $|e\rangle$ is lowered into the lower energy state of the qubit $|g\rangle$ by emmitting a quantum of energy. The rate at which this occurs is referred to as T_1.

PHOTON LOSS

Photon loss is the process in which the Fock state $|n\rangle$ loses a quantum of energy (a photon) and is lowered into the state $|n-1\rangle$, corresponding to applying the photon annihilation operator $\hat{a}$ to the state of the system at a certain rate. Photon loss occurs more rapidly for higher energy states of the system. This is a non unitary evolution of the quantum state which causes decoherence.

Dephasing, relaxation and photon loss are all examples of decoherence that introduce a non unitary evolution in the QRW which disturbs the quantum mechanical properties of the QRW such as interference.

COHERENCE TIMES

For a transmon qubit previous research has shown that $T_1 = 50\mu s$ and $T_2 = 60\mu s$. [17] In this research a controlled displacement followed by transmon readout is performed in approximately 1.1 μs. Considering that the sequence in Figure 4.3 consists of 2 controlled displacements and 2 Hadamard gates, but no transmon readout, it seems promising that about $O(10) - O(100)$ steps of the described 2D walk with the sequence in Figure 4.3 are realizable with superconducting qubits in circuit-QED.

5.2. SUGGESTIONS FOR FURTHER RESEARCH

In this thesis the implementation of a QRW on a 2D grid in phase space using controlled displacements has been studied. A theoretical setup is given and a numerical simulation for different sizes of the grid has been performed. There are a few open questions remaining that are interesting to study in further research.

We shortly discussed the effect of dephasing, relaxation and photon loss on the QRW on a 2D grid in phase space. It would be interesting to investigate these decoherence effects further in future research to see if a realization of a QRW in the suggested setup would indeed be reliable, for example by implementing these effects into the numerical model. Exploring the possibilities for an experimental setup of the suggested sequence in Figure 4.3 would also be interesting for further research.

In the suggested setup, the 2D walk was performed on a 2D rectangular grid. It might be interesting to research a possible setup for a hexagonal grid, using a qutrit for the three directions in which the walk can move at every point of the grid. This might also result in interesting properties of the 2D QRW with different interference patterns. A difficulty with a hexagonal grid might be the asymmetry of the directions in which the walk can move at different points of the grid. The choice for two Hadamard gates on each of the qubits in our suggested setup could perhaps also be extended to a two-qubit gate that creates a more entangled coin state for the 4 directions in which the walk moves at each step. Perhaps this makes it possible to create a more entangled 2D walk that does not consist of two uncoupled 1D walks.

We observed that the 2D QRW on the grid is actually composed of two uncoupled 1D QRW's. This creates a rectangular shaped probability distribution on the grid for the

commuting 2D QRW. This is different compared to the circular distribution that appears for a 2D CRW. In the classical case, the probability amplitude corresponding to a position at a certain distance from the origin is invariant under the direction on the 2D grid of this position. An interesting question that remains is whether it is possible to design a 2D QRW that has this same property. It seems that in phase space this is difficult, since $\hat{p}$ and $\hat{x}$ do not commute. Perhaps it is possible to use the circular shaped distribution that arises before the collapse of some of the non-commuting walks we investigated to create a 2D QRW with this property. This idea might be further researched and is beyond the scope of this thesis.

In Chapter 2 we shortly named a few applications of the QRW in quantum algorithms. In further research it might be interesting to investigate the possibilities for applying the suggested 2D QRW in phase space in algorithms such as a 2D quantum grid search with a marked item.

Finally, further research on mathematical proofs and explanations of our observations of the 2D QRW is recommended to understand more about the behaviour of these 2D QRW's on a grid in phase space. Further investigation on QRW's in our setup for simulations longer than $t = 100$ steps might be necessary to find out more about the collapse that occurs for some values of $\alpha \cdot \beta$.

6

CONCLUSION

In this research, implementation of a discrete QRW on the Fock states of the quantum harmonic oscillator, and implementations of a discrete QRW on a 2D grid of coherent states in phase space with superconducting circuit-QED were studied.

A 1D QRW on the Fock states of a harmonic oscillator by using a Jaynes-Cummings model was investigated. A problem with this idea is the n-dependency of the frequency Ω_n of the Rabi Oscillations. The theoretical effect of the lower boundary induced by the ground state $|0\rangle$ of the harmonic oscillator was investigated. The probability amplitudes are reflected backwards at the boundary, in contrast to a 1D QRW on an infinite line.

A setup of a 1D and 2D QRW on a grid in phase space was suggested, using controlled displacements of a resonator dispersively coupled to one or two superconducting transmon qubits in circuit-QED, followed by Hadamard gates. Previous research has shown that controlled displacements are physically realizable with decent control in circuit-QED. Properties of the results of numerical simulations of these walks were investigated. For the 2D QRW on the rectangular grid of coherent states $|n\alpha + im\alpha\rangle$, it was observed that the walk is equal to two uncoupled 1D QRW's for values of α and β when $\alpha \cdot \beta = 0 \mod \pi$, because the horizontal and vertical displacements commute. From numerical simulations it seemed that the displacements also commute for $\alpha \cdot \beta = 0 \mod \frac{\pi}{2}$. For other values of $\alpha \cdot \beta$ the horizontal and vertical displacements do not commute, resulting in a different pattern of the QRW. From numerical simulations of these noncommuting 2D QRW's it seemed that this pattern was equal for QRW's with different values of $\alpha \cdot \beta$ of equal distance $|\alpha \cdot \beta - 0 \mod \frac{\pi}{2}|$.

For values closer to $0 \mod \frac{\pi}{2}$ than 0.01 the QRW is very similar to the commuting QRW. A possible explanation for this is that the phase factors introduced by non-commutativity of the controlled displacements are small. The phases do not accumulate to a collapse of the quantum interference effect within $t = 100$ steps of the walk.

For most values of $\alpha \cdot \beta$ with a larger distance to 0 mod $\frac{\pi}{2}$ we see that the probability distribution of the walk collapses to a distribution centered around origin within $t = 100$ steps. The variance of the x-coordinate of these walks is similar to or sometimes even smaller than the CRW and no clear relationship between the variance and the number of steps t is found. Exceptions are the 2D QRW's for $\alpha \cdot \beta = \pm\frac{\pi}{6}$ mod $\frac{\pi}{2}$ or $\pm\frac{\pi}{4}$ mod $\frac{\pi}{2}$, which still show proportionality $\sigma_x^2 \sim t^2$. A possible explanation for this is that the phase factors introduced by non-commutativity add up to integer multiples of π, causing the quantum interference not to disappear completely.

For further research it is recommended that decoherence effects such as dephasing, relaxation and photon loss in the 2D QRW in phase space are taken into account. A modification of our setup for a hexagonal grid instead of a rectangular grid, or a modification of the 2 Hadamard gates to a two-qubit gate might also introduce interesting properties of the 2D QRW. Investigation of the possibility of designing a 2D QRW that behaves similarly to the 2D CRW in the sense that the probability distribution is circularly symmetric is suggested. Perhaps the non-commuting 2D QRW's that were studied, which transfer from a rectangular to a circular shape before collapsing to a distribution centered around the origin, could be used to do this. Further study of the possibility for applications in quantum algorithms of the 2D QRW in phase space is also suggested.

Finally, further research on mathematical proofs and explanations of our observations of the 2D QRW's on a grid in phase space is recommended to understand more about the behaviour of these walks. This also includes further investigation on 2D QRW's in our setup for simulations longer than $t = 100$ steps.

BIBLIOGRAPHY

[1] F. et al. Xia. “Quantum Walks on Graphs”. In: (2020). URL: https://arxiv.org/abs/2008.03639.

[2] D. Aharonov. “Quantum random walks”. In: (1993). URL: https://journals.aps.org/pra/abstract/10.1103/PhysRevA.48.1687.

[3] A. Blais et al. “Circuit Quantum Electrodynamics”. In: *Rev. Mod. Phys* 93 (2020). URL: https://arxiv.org/abs/2005.12667.

[4] G. Grimmett and D. Welsh, eds. *Probability, An Introduction*. Oxford University Press, 2014. ISBN: 978-0-19-870997-8.

[5] D. Ahanorov, A. Ambainis, and J. Kempe. “Quantum Walks on Graphs”. In: *Proceedings of ACM Symposium on Theory of Computation* (2001), pp. 50–59. URL: https://arxiv.org/abs/quant-ph/0012090.

[6] L. Page et al. *The PageRank Citation Ranking: Bringing Order to the Web*. Tech. rep. Stanford InfoLab, 1999. URL: http://ilpubs.stanford.edu:8090/422/.

[7] D. Aldous and P. Diaconis. “Shuffling Cards and Stopping Times”. In: *The American Mathematical Monthly* 93.2 (1986), pp. 333–348. URL: https://doi.org/10.1080/00029890.1986.11971821.

[8] D.J. Griffiths, ed. *Introduction to Quantum Mechanics*. Prentice Hall, New Jersey, 1995, pp. 1–44. ISBN: 0-13-124405-1.

[9] M.A. Nielsen and I.L. Chuang, eds. *Quantum Computation and Quantum Information*. Cambridge University Press, 2000. ISBN: 0-521-63503-9.

[10] J. Kempe. “Quantum Random Walks - an introductory overview”. In: *Contemporary Physics* 44.4 (2003), pp. 307–327. URL: https://arxiv.org/abs/quant-ph/0303081.

[11] G.D. Paparo et al. “Quantum Google in a Complex Network”. In: *Scientific Reports* 2773 (2013). URL: https://www.nature.com/articles/srep02773.

[12] C.C Gerry and P.L Knight, eds. *Introductory Quantum Optics*. Cambridge University Press, 2005, pp. 10–18, 90–99. ISBN: 978-0-511-22949-7.

[13] S. Haroche and J.M. Raimond, eds. *Exploring the Quantum, Atoms, Cavities, and Photons*. Oxford University Press, 2006. ISBN: 0-19-850912-6.

[14] P Xue, B.C. Sanders, and D Leibfried. “Quantum walk on a line for a trapped ion”. In: *Phys. Rev. Lett.* 103 (2009). URL: https://arxiv.org/abs/0904.1451v2.

[15] P Xue et al. “Quantum walks on circles in phase space via superconducting circuit quantum electrodynamics”. In: *Physical Review A* 78 (2008). DOI: 10.1103/PhysRevA.78.042334. URL: https://arxiv.org/abs/0802.2750v2.

[16] Ming Gong et al. “Quantum walks on a programmable two-dimensional 62-qubit superconducting processor”. In: *Science* 372.6545 (2021), pp. 948–952. URL: https://science.sciencemag.org/content/372/6545/948.

[17] P. Campagne-Ibarcq, A. Eickbusch, and S. Touzard. “Quantum error correction of a qubit encoded in grid states of an oscillator.” In: *Nature* 584 (2020), pp. 368–372. URL: https://doi.org/10.1038/s41586-020-2603-3.

[18] D. Weignand. “Encoding a Qubit into an Oscillator with Near-Term Experimental Devices”. In: (2020). URL: https://doi.org/10.4233/uuid:72abf99f-dd2d-42a1-8c59-7a83870c9d3c.

[19] K. Motes, A. Gilchrist, and P. Rohde. “Quantum random walks on congested lattices and the effect of dephasing.” In: *Scientific Reports* 6 (2016). URL: https://www.nature.com/articles/srep19864.

[20] A. Alberti et al. “Decoherence models for discrete-time quantum walks and their application to neutral atom experiments”. In: *New Journal of Physics* 16 (2014). URL: https://doi.org/10.1088/1367-2630/16/12/123052.

A

APPENDIX: LINK TO NUMERICAL CODE

The written code used for numerical simulations organised by chapter of the thesis is available at https://github.com/adijkhorst/BEP-QRW.git.